Airmass Origin in the Arctic. Part I: Seasonality

CLARA ORBE,* PAUL A. NEWMAN,* DARRYN W. WAUGH,+ MARK HOLZER,#,@ LUKE D. OMAN,* FENG LI,& AND LORENZO M. POLVANI#,**

* *Laboratory for Atmospheric Chemistry and Dynamics, NASA Goddard Space Flight Center, Greenbelt, Maryland*
+ *Department of Earth and Planetary Sciences, Johns Hopkins University, Baltimore, Maryland*
# *Department of Applied Mathematics, School of Mathematics and Statistics, University of New South Wales, Sydney, New South Wales, Australia*
@ *Department of Applied Physics and Applied Mathematics, Columbia University, New York, New York*
& *Goddard Earth Sciences Technology and Research, Universities Space Research Association, Columbia, Maryland*
** *Lamont Doherty Earth Observatory, Columbia University, Palisades, New York*

(Manuscript received 21 October 2014, in final form 15 March 2015)

ABSTRACT

The first climatology of airmass origin in the Arctic is presented in terms of rigorously defined airmass fractions that partition air according to where it last contacted the planetary boundary layer (PBL). Results from a present-day climate integration of the Goddard Earth Observing System Chemistry–Climate Model (GEOSCCM) reveal that the majority of air in the Arctic below 700 mb last contacted the PBL poleward of 60°N. By comparison, 62% (±0.8%) of the air above 700 mb originates over Northern Hemisphere midlatitudes (i.e., "midlatitude air"). Seasonal variations in the airmass fractions above 700 mb reveal that during boreal winter air from midlatitudes originates primarily over the oceans, with 26% (±1.9%) last contacting the PBL over the eastern Pacific, 21% (±0.87%) over the Atlantic, and 16% (±1.2%) over the western Pacific. During summer, by comparison, midlatitude air originates primarily over land, overwhelmingly so over Asia [41% (±1.0%)] and, to a lesser extent, over North America [24% (±1.5%)]. Seasonal variations in the airmass fractions are interpreted in terms of changes in the large-scale ventilation of the midlatitude boundary layer and the midlatitude tropospheric jet.

1. Introduction

Long-range transport from midlatitudes plays a key role in setting the distributions of trace species and aerosols in the Arctic (e.g., Raatz and Shaw 1984; Barrie 1986). Aircraft observations going back several decades, for example, have shown that during late winter and early spring there is a significant buildup of midlatitude aerosols in the Arctic, often referred to as "Arctic haze" (e.g., Mitchell 1957; Rahn and McCaffrey 1980). More recently, studies have also linked high levels of black carbon in the Arctic during summer to boreal forest fires that occur at midlatitudes (e.g., Stohl 2006; Law and Stohl 2007).

Understanding how constituents are transported from Northern Hemisphere (NH) midlatitudes into the Arctic becomes ever more pressing in light of strong evidence that Arctic composition affects climate. Increases in aerosols, for example, have increased surface longwave fluxes over the Arctic by an average of 3.4 $W m^{-2}$ in recent decades by altering the microphysical properties of clouds (Hansen and Nazarenko 2004; Lubin and Vogelmann 2006; Garrett and Zhao 2006). Still other constituents affect climate through photochemistry, with decades' worth of observations showing that the wintertime buildup of halocarbons of midlatitude origin in the Arctic unequivocally leads to rapid ozone production during spring (Atlas et al. 2003; Klonecki et al. 2003). Therefore, a comprehensive understanding of the seasonally varying transport from NH midlatitudes to the Arctic is key for understanding climate.

The distributions of trace species in the Arctic are ultimately determined by the complex interplay of their emissions, chemistry, and transport. Hence, disentangling transport from species' emissions patterns and chemistry is important for our understanding, and accurate modeling, of Arctic composition. However, while transport uncertainties have led to significant spread

Corresponding author address: Clara Orbe, Laboratory for Atmospheric Chemistry and Dynamics, NASA Goddard Space Flight Center, Greenbelt, MD 20771.
E-mail: clara.orbe@nasa.gov

DOI: 10.1175/JCLI-D-14-00720.1

among modeled distributions of carbon monoxide and ozone (Shindell et al. 2008), there have been few rigorous efforts to understand these uncertainties, largely because diagnostics that can parse out the underlying transport are lacking.

Transport uncertainties become still more concerning when making projections of the future distributions of chemical species, whose emissions and chemical lifetimes will also change as the large-scale atmospheric circulation responds to future warming. And yet, while the climate changes in atmospheric patterns have been assessed in terms of changes in the position and strength of the midlatitude tropospheric jets (e.g., Yin 2005; Miller et al. 2006; Barnes and Polvani 2013), changes in the frequency and intensity of extratropical cyclones (e.g., Hoskins and Hodges 2002; Bengtsson et al. 2006; Lambert and Fyfe 2006; Bengtsson et al. 2009; Catto et al. 2011; Chang et al. 2012), and changes in the strength and width of the Hadley cell (e.g., Lu et al. 2007; Seidel et al. 2007), relatively little attention has been paid to assessing the large-scale transport response in the Arctic.

A natural approach to quantifying transport into the Arctic is using tracers that capture a fundamental aspect of the atmosphere's advective eddy-diffusive transport operator, independent of any particular trace species (i.e., herein referred to as "tracer independent"). Here we focus on the spatial distribution of rigorously defined air masses in the Arctic, which are defined with respect to their origin in the planetary boundary layer (PBL). More precisely, the PBL airmass fraction at point **r**, whose PBL origin was in the geographic region Ω_i, is simply defined as the mass fraction of the air at **r** that had its last contact with the PBL in region Ω_i, as shown schematically in Fig. 1.

In practice, airmass fractions are calculated as equilibrated tracer mixing ratios with boundary conditions specified so that they reveal where in the Arctic, and with what dilution, the air from various sources can be found. A simple application of the concept of airmass fractions to the atmosphere was performed by Orbe et al. (2013) using a dynamical core general circulation model (GCM) for the purposes of assessing the airmass origin response to an idealized warming that mimicked the response of comprehensive climate models to end-of-twenty-first-century warming (Meehl et al. 2007; Wang et al. 2012). The climate of the dynamical core circulation and its responses to a prescribed heating were ideal for the purposes of illustrating the utility of airmass fractions as diagnostics of tropospheric transport. Here, we extend the approach developed in that study to examine seasonal variations in Arctic airmass origin using a comprehensive climate model.

Our goals are twofold: 1) to construct a baseline Arctic "transport climate" (Holzer and Hall 2000; Holzer and Boer 2001) in terms of airmass origin and 2) to assess the response of airmass origin in the Arctic to future warming. In this study we address the first goal by presenting model climatologies of airmass origin for boreal winter and summer, calculated from a time-slice integration of the Goddard Earth Observing System Chemistry–Climate Model (GEOSCCM) subject to atmospheric forcings representative of the current climate. In the second part of this study to be published, we will assess the airmass response to future warming using a separate time-slice integration of GEOSCCM forced with future greenhouse gases and ozone-depleting substances.

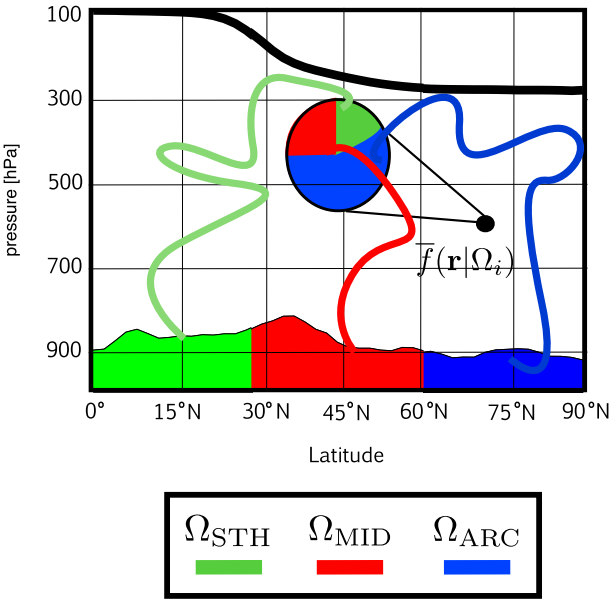

FIG. 1. Schematic illustration of the PBL airmass fractions $\overline{f}(\mathbf{r}\,|\,\Omega_i)$. The thick black line indicates the DJF climatological mean thermal tropopause. The airmass fractions partition air at point **r** according to where last contact occurred with the planetary boundary layer (PBL). Shown here, for illustrative purposes, are the PBL Ω_i regions of fixed zonal width, Ω_{STH} (green), Ω_{MID} (red), and Ω_{ARC} (blue), which are illustrated using the DJF climatological mean PBL. Note that the horizontal axis is restricted to the Northern Hemisphere (NH).

Following a brief exposition of the theory and methodology in sections 2 and 3, we present the airmass origin climatologies in section 4. The interpretation of the airmass fractions in terms of the large-scale circulation is reserved for section 5, followed by discussions and conclusions in sections 6 and 7, respectively.

2. Theory of airmass fractions

To identify where Arctic air last contacted the PBL, we first we subdivide the PBL volume, denoted by Ω, into smaller geographic regions Ω_i (e.g., zonal strips of fixed width; see section 3b for a description of the

regions used here). By definition, the mass fraction that had last contact with the PBL in region Ω_i, and not elsewhere, is equal to unity in Ω_i and equal to zero in the complement of Ω_i (the rest of Ω), denoted by Ω_i^c (Orbe et al. 2013).

In practice, the airmass fraction is calculated as the interior mixing ratio of a passive tracer f that is in statistical equilibrium with boundary conditions of $f = 1$ in Ω_i and $f = 0$ in Ω_i^c, without any other sources or sinks. By labeling a fluid element (i.e., "particle") when it is in Ω_i as being 100% Ω_i PBL air, and removing this label (setting it to zero) as soon as the particle finds itself in the PBL outside of Ω_i, the boundary conditions ensure that $f(\mathbf{r}, t \,|\, \Omega_i)$ is the mass fraction of air that had last contact with the PBL on Ω_i and not elsewhere (Orbe et al. 2013). Formally, f is computed as the solution to the passive tracer advection–diffusion equation

$$(\partial_t + \mathcal{T}) f(\mathbf{r}, t \,|\, \Omega_i) = 0, \tag{1}$$

where $\mathcal{T}$ denotes the linear advection–diffusion transport operator, which in a model context includes parameterized subgrid-scale processes such as convection. At the PBL (i.e., for all points $\mathbf{r}_\Omega \in \Omega$) the fraction f satisfies the boundary condition

$$f(\mathbf{r}_\Omega, t \,|\, \Omega_i) = \Delta(\mathbf{r}_\Omega, \Omega_i), \tag{2}$$

where $\Delta(\mathbf{r}_\Omega, \Omega_i) = 1$ if $\mathbf{r}_\Omega \in \Omega_i$ and $\Delta(\mathbf{r}_\Omega, \Omega_i) = 0$ if $\mathbf{r}_\Omega \in \Omega_i^c$.

The boundary conditions on f ensure that the sum of the fraction is always held at unity over the entire PBL so that, after all initial conditions have decayed, the sum of the fractions must be equal to the boundary value throughout the entire atmosphere. By construction, therefore, when equilibrium with the boundary conditions has been reached, the airmass fractions satisfy

$$\sum_{\Omega_i} f(\mathbf{r}, t \,|\, \Omega_i) = 1 \tag{3}$$

at every point $\mathbf{r}$ and time t. Physically, Eq. (3) states that the air at $(\mathbf{r}, t)$ had to have last contacted the PBL somewhere in its history and provides a useful numerical check for whether equilibrium has been reached.

3. Experimental design

a. The model

We use GEOSCCM version 2, which is an update from the GEOSCCM version 1 (Pawson et al. 2008) and couples the GCM GEOS-5 (Rienecker et al. 2008) with a comprehensive stratospheric chemistry package (Douglass et al. 1996). The model has a horizontal resolution of 2° latitude by 2.5° longitude, with 72 vertical levels extending from the surface to 0.01 mb (1 mb = 1 hPa). Airmass fractions are calculated from one integration of the model forced with annually repeating 2000–19 time-averaged greenhouse gases (GHGs) and ozone-depleting substances (ODSs) under the SRES A1B and A1 scenarios, respectively (Houghton et al. 2001; WMO 2007). Sea surface temperatures and sea ice concentrations are 2000–19 time averages taken from an integration of the NCAR Community Climate System Model 3.0 subject to A1B GHG forcing. Solar forcings are held constant, and there is no representation of the quasi-biennial oscillation (QBO).

Spinup to a statistically stationary state for the dynamical variables (not the tracers) takes 10 years, after which we introduce our diagnostic tracers that are passively advected for an additional 20 years using a flux-form semi-Lagrangian transport scheme (Lin and Rood 1996). As in most GCMs, convective transport is realized both on resolved scales by the large-scale flow and through subgrid-scale processes that are parameterized using the relaxed Arakawa–Schubert convective scheme (Moorthi and Suarez 1992), a modified version of the original Arakawa–Schubert scheme (Arakawa and Schubert 1974). There is no explicit diffusion applied to tracers either in the horizontal or vertical.

Airmass origin regions are defined with respect to the model's PBL, which is calculated online as the height of the lowest model layer in which the total eddy diffusion coefficient of heat falls below $2\,\mathrm{m^2\,s^{-1}}$. Overall, the modeled PBL agrees well with summertime and wintertime climatologies of PBL height derived from reanalysis (von Engeln and Teixeira 2013) by capturing gross height differences between land and ocean, as well as smaller-scale features, including wintertime minima over Canada and Greenland and summertime maxima over the west coast of the United States (see appendix Fig. A1). Owing to underlying model biases in surface sensible heat fluxes, however, the modeled PBL tends to be too high in summer, compared to independent radiosonde-based estimates of PBL height (McGrath-Spangler and Molod 2014). As discussed in section 6, however, we do believe that this bias significantly affects the qualitative nature of our findings.

To preface the exposition of the airmass fractions in section 4, we first briefly describe the modeled large-scale circulation in the NH extratropics. Seasonal mean climatologies of the 300–900-mb column-integrated zonal winds (Fig. 2a) provide a gross sense for the position of the storm tracks and warm conveyer belts (hence, the ventilation of the midlatitude boundary layer) and reveal that during winter the midlatitude jet is strongest over the Pacific Ocean and over the Atlantic Ocean, where it extends back

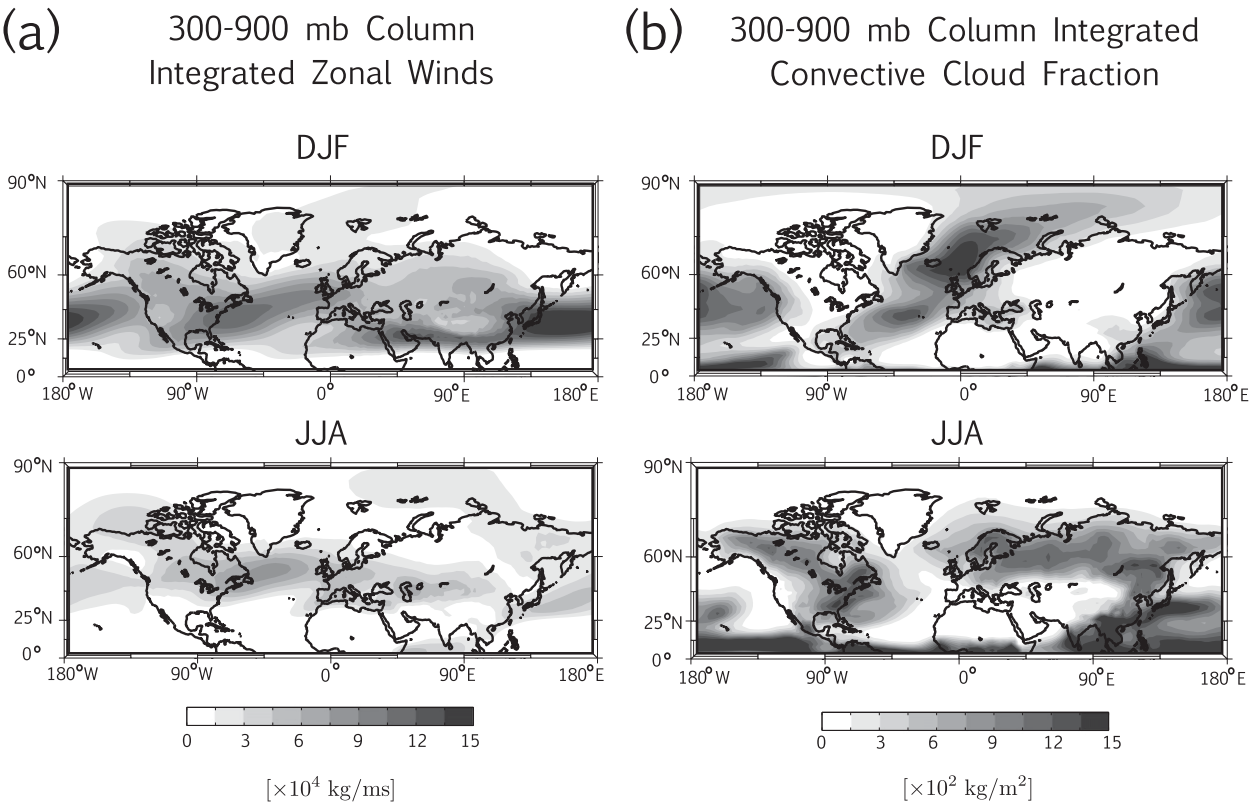

FIG. 2. (a) Seasonally averaged climatological mean zonal winds, column integrated over the free troposphere (300–900 mb) for (top) DJF and (bottom) JJA. (b) As in (a), but for the convective cloud fraction, which is used throughout as a proxy for large-scale ascent over NH midlatitudes.

to the central United States and over Europe (Fig. 2a, top). By comparison, during summer the jet is relatively weaker and maximizes over the Atlantic Ocean and western Europe (Fig. 2a, bottom).

It is important to note that although the modeled zonal winds at 300 mb compare well with the ensemble mean among comprehensive climate models participating in phases 3 and 5 of CMIP (CMIP3 and CMIP5, respectively; Delcambre et al. 2013; Barnes and Polvani 2013), significant intermodel spread renders the ensemble mean not truly representative of any single model or the observed climate. In particular, like most GCMs, GEOS-5 tends to overestimate the seasonal cycle of jet latitude about its mean, with the midlatitude jet positioned too far equatorward and poleward during December–February (DJF) and June–August (JJA), respectively (Molod et al. 2012). Consistent with the other CMIP5 models, these biases are largest in the North Atlantic and the Southern Hemisphere (Barnes and Polvani 2013).

While the tropospheric jet crudely constrains the ventilation of the midlatitude boundary layer during winter, the summertime distribution of convective clouds provides a gross sense for the large-scale vertical motions over midlatitudes that is preferable to other diagnostics that are inherently noisier and more difficult to interpret (i.e., the vertical velocity ω). Large-scale convection is concentrated at midlatitudes over land during summer (Fig. 2b, bottom), particularly over North America and Eurasia, where large cloud fractions span the poleward and southward edges of Asia.

By comparison, the wintertime convective cloud fraction pattern aligns broadly with the Pacific and North Atlantic storm tracks (Fig. 2b, top). Large cloud fractions over the Norwegian Sea are collocated with an anomalously high PBL during winter (Fig. A1) and therefore most likely reflect the strong surface winds in that region that stem from the deformation of the Atlantic jet by high topography over Greenland (Moore and Renfrew 2005; Moore 2012). These detailed features aside, convective cloud fraction is mainly interpreted throughout as a qualitative measure of the large-scale vertical motions in the extratropics.

b. The diagnostic tracers

We first partition the PBL into three zonally symmetric origin regions Ω_i, the colored bands shown in Fig. 3a. The Ω_i consist of a "southern latitude patch" (Ω_{STH}) spanning latitudes south of 25°N, a "midlatitude

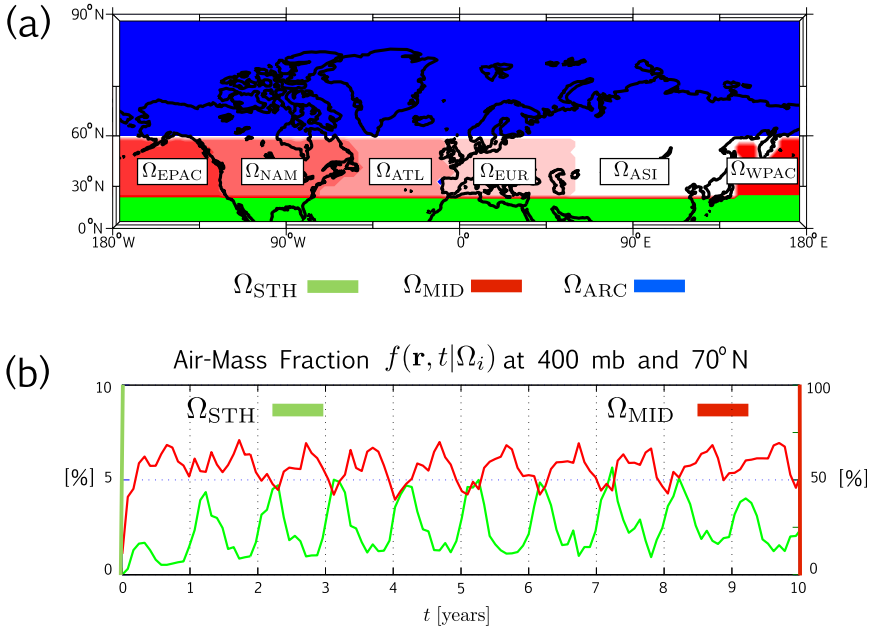

FIG. 3. (a) The Ω_i regions where airmass fractions in the Arctic last contacted the PBL. Zonal strips of fixed width span the NH midlatitudes over 25°–60°N (Ω_{MID}, red), latitudes to the south of Ω_{MID} from 90°S to 25°N (Ω_{STH}, green), and latitudes to the north of Ω_{MID} poleward of 60°N (Ω_{ARC}, blue). Red colored patches indicate the regions where Ω_{MID} has been further partitioned between the EPAC, NAM, ATL, EUR, ASI, and the WPAC. (b) The evolution of the zonal mean fraction $f(\mathbf{r}, t \mid \Omega_i)$ evaluated at 400 mb and 70°N for air that last contacted the PBL over Ω_{MID} (red) and over Ω_{STH} (green). Annually and seasonally averaged airmass fraction climatologies are presented in the following figures and have been calculated over model years 10–20 (i.e., post equilibrium).

patch'' (Ω_{MID}) between 25° and 60°N, and an ''Arctic patch'' (Ω_{ARC}) poleward of 60°N. In addition, we further subdivide Ω_{MID} into six nonoverlapping origin regions over the eastern Pacific, North America, the Atlantic, Europe, Asia, and the western Pacific, which, for convenience, are referred to throughout using the labels EPAC, NAM, ATL, EUR, ASI, and WPAC, respectively. These regions have been defined in order to distinguish between last-PBL contact over land and ocean as well as to broadly identify regions of high industrial emissions (hence the separation of the Eurasian continent into Ω_{EUR} and Ω_{ASI}).

In total, we carry nine passive airmass fraction tracers $f(\mathbf{r}, t \mid \Omega_i)$, one for each Ω_i region. Tracers are integrated for 20 years after the dynamical variables are spun up to climatology in order to ensure that equilibrium has been reached everywhere in the Arctic [i.e., Eq. (3) is satisfied]. In particular, the long integration time accommodates air that receives its origin label over Ω_{STH} and takes approximately 2–3 years to reach a statistically stationary state in the Arctic, much longer than the equilibration time for the Ω_{MID} airmass fraction (Fig. 3b). (As shown in section 4a, this 2–3-yr time scale reflects the fact that air that is first labeled at Ω_{STH} passes through the lower stratosphere en route to the Arctic.) Once air masses have reached equilibrium, their annual (ANN), wintertime (DJF), and summertime (JJA) climatological mean fractions are calculated over the last 10 years of the integration, and are denoted as $\overline{f}^{ANN}(\mathbf{r} \mid \Omega_i)$, $\overline{f}^{DJF}(\mathbf{r} \mid \Omega_i)$, and $\overline{f}^{JJA}(\mathbf{r} \mid \Omega_i)$. Hereafter all 10-yr climatologies are denoted using an overbar.

For convenience, the airmass fraction corresponding to the region Ω_i will be referred throughout as ''Ω_i air.'' Note that the term ''origin'' is used throughout in reference to the region where air last contacted the PBL. For example, ''Ω_{STH} air'' (also southern air or air of southern origin) will refer to the airmass fraction at $\mathbf{r}$ that last encountered the PBL south of 25°N. Finally, in order to keep Ω_i physically meaningful, we have not constrained the Ω_i airmass origin regions over midlatitudes to be equal in surface area. However, separate calculations, in which the airmass fractions have first been normalized by the area of their origin region, show that, qualitatively, our results do not hinge on patch size.

4. Origins of Arctic air masses

We now examine systematically the climatological airmass fractions $\overline{f}^{ANN}(\Omega_i)$, $\overline{f}^{DJF}(\Omega_i)$, and $\overline{f}^{JJA}(\Omega_i)$. First we present the airmass fractions that last contacted the

PBL over $\Omega_{\rm STH}$, $\Omega_{\rm MID}$, and $\Omega_{\rm ARC}$. We then examine the $\Omega_{\rm MID}$ airmass fraction in more detail, further distinguishing between last PBL contact at midlatitudes over land and over ocean. Because the budgets for spring [March–May (MAM)] and fall [September–November (SON)] are found to be, approximately, interpolations between NH winter and summer, the airmass fractions are only presented for DJF and JJA. Seasonal variations in the airmass fractions are then interpreted in section 5 in terms of the large-scale circulation. Throughout, statistical significance in the airmass fractions is quantified using the standard deviation $\sigma_{\bar{f}}(\mathbf{r}\,|\,\Omega_i) \equiv \{N^{-1}\sum_{n=1}^{N}[\tilde{f}_n(\mathbf{r}\,|\,\Omega_i) - \bar{f}(\mathbf{r}\,|\,\Omega_i)]^2\}^{1/2}$, where $N = 10$ and $\tilde{f}_n(\mathbf{r}\,|\,\Omega_i)$ denotes the (ANN, DJF, or JJA) average of $f(\mathbf{r}, t\,|\,\Omega_i)$ in year n within the last 10 years of the integration. (Significance is denoted throughout using $\pm\sigma_{\bar{f}}$ notation.)

a. *Origin over* $\Omega_{\rm STH}$, $\Omega_{\rm MID}$, *and* $\Omega_{\rm ARC}$

Vertical profiles of the annually averaged airmass fractions in the Arctic, $\bar{f}^{\rm ANN}_{\rm ARC}(p\,|\,\Omega_{\rm STH})$, $\bar{f}^{\rm ANN}_{\rm ARC}(p\,|\,\Omega_{\rm MID})$, and $\bar{f}^{\rm ANN}_{\rm ARC}(p\,|\,\Omega_{\rm ARC})$ (Fig. 4), reveal that the air in the Arctic free troposphere (i.e., 300–900 mb) originates primarily over $\Omega_{\rm ARC}$ and over $\Omega_{\rm MID}$. (The subscript ARC denotes the average over latitudes poleward of 60°N.) Note that, because $\Omega_{\rm STH}$, $\Omega_{\rm MID}$, and $\Omega_{\rm ARC}$ span the entire PBL (Ω), Eq. (3) ensures that the sum of their corresponding $\bar{f}^{\rm ANN}_{\rm ARC}(p\,|\,\Omega_i)$ equals 100% at each pressure level.

The $\Omega_{\rm ARC}$ and $\Omega_{\rm MID}$ airmass fractions make roughly equal contributions to the Arctic free troposphere [40% (±0.87%) and 51% (±0.70%), respectively]. Differences in the vertical profiles of $\bar{f}^{\rm ANN}(\mathbf{r}\,|\,\Omega_{\rm ARC})$ and $\bar{f}^{\rm ANN}(\mathbf{r}\,|\,\Omega_{\rm MID})$, however, reveal that 70% of the air below 700 mb (hereafter referred to as the "lower Arctic") last contacted the PBL over $\Omega_{\rm ARC}$, while the majority of air [62% (±0.82%)] in the "middle Arctic" (i.e., 300–700 mb) originated over NH midlatitudes. Interestingly, there is a surprisingly large (~12%) contribution of southern air in the middle Arctic.

Climatologies performed separately for DJF and JJA reveal that the annual mean and column integrated balance of $\Omega_{\rm STH}$, $\Omega_{\rm MID}$, and $\Omega_{\rm ARC}$ air in the Arctic is to first order unchanged between boreal winter and summer (Table 1). Nonetheless, there are large seasonal variations within the troposphere, especially above 700 mb, where air is approximately 11% less likely to last have contacted the PBL in the Arctic during winter compared to summer.

Seasonal variations are more easily interpreted by comparing the zonal mean distributions of $\bar{f}^{\rm DJF}(\mathbf{r}\,|\,\Omega_i)$ and $\bar{f}^{\rm JJA}(\mathbf{r}\,|\,\Omega_i)$, which reveal that during boreal winter $\bar{f}^{\rm DJF}(\mathbf{r}\,|\,\Omega_{\rm ARC})$ is more or less confined to pressures below 500 mb (Fig. 5, top left). During boreal summer, by

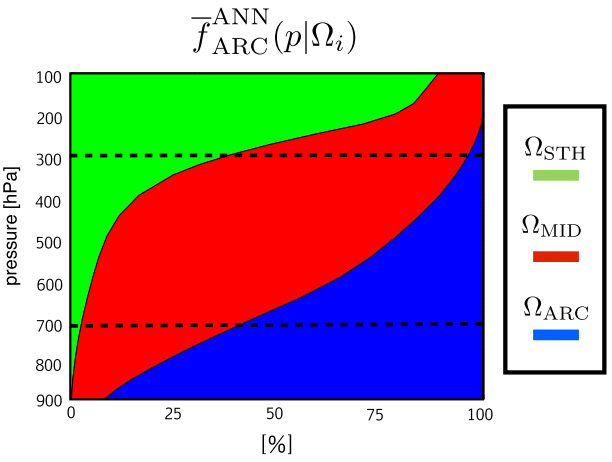

FIG. 4. Vertical profiles of the annual mean climatological mass fraction of the Arctic that last contacted the PBL over Ω_i, $\bar{f}^{\rm ANN}_{\rm ARC}(p\,|\,\Omega_i)$, where the subscript ARC denotes the average over latitudes poleward of 60°N. Profiles are shown for the origin regions $\Omega_{\rm STH}$ (green), $\Omega_{\rm MID}$ (red), and $\Omega_{\rm ARC}$ (blue). The black dashed lines at 700 and 300 mb, respectively, bound the lower and middle Arctic.

comparison, contours of $\bar{f}^{\rm JJA}(\mathbf{r}\,|\,\Omega_{\rm ARC})$ extend into the upper troposphere as warmer Arctic temperatures and reduced stability at the surface enhance the rate with which $\Omega_{\rm ARC}$ air is mixed away from the boundary layer (Fig. 5, top right).

For both winter and summer the $\Omega_{\rm ARC}$ airmass fraction is flanked aloft by $\bar{f}(\mathbf{r}\,|\,\Omega_{\rm MID})$ (Fig. 5, middle panels), effectively rendering the lower Arctic a "polar dome" (Klonecki et al. 2003; Law and Stohl 2007). During winter, contours of $\bar{f}^{\rm DJF}(\mathbf{r}\,|\,\Omega_{\rm MID})$ indicate that transport away from the midlatitude PBL occurs primarily along isentropes, although there is some suggestion of cross-isentropic transport over the pole, induced by diabatic cooling. Independent analysis reveals that this flattening of contours does not merely reflect changes in the isentropes overlying the Arctic, although this is not shown, for sake of brevity.

During summer there is less air of midlatitude origin in the Arctic, as contours of $\bar{f}^{\rm JJA}(\mathbf{r}\,|\,\Omega_{\rm MID})$ penetrate across isentropes into the upper subtropical and midlatitude troposphere (Fig. 5, middle right). In particular, the airmass fraction at the equatorward edge of $\Omega_{\rm MID}$ is steered into the subtropical upper troposphere by the upwelling branch of the summertime Hadley cell, by which we mean the zonally averaged meridional overturning circulation in the tropics and subtropics, overlaid in Fig. 5 (bottom panels) in terms of the streamfunction.

Still stronger signatures of upwelling associated with the Hadley cell appear in the distributions of $\bar{f}^{\rm DJF}(\mathbf{r}\,|\,\Omega_{\rm STH})$ and $\bar{f}^{\rm JJA}(\mathbf{r}\,|\,\Omega_{\rm STH})$ (Fig. 5, bottom panels), which account for a surprisingly large (>10%) fraction of air in the Arctic

TABLE 1. The DJF and JJA climatological mean fraction of the Arctic that last contacted the PBL over Ω_{ARC}, Ω_{MID}, and Ω_{STH}. Airmass fractions corresponding to the Ω_i origin regions have been averaged over latitudes poleward of 60°N (hence, the subscript ARC) and column integrated over the free troposphere (300–900 mb; column 2), the lower troposphere (700–900 mb; column 3), and the middle-to-upper troposphere (300–700 mb; column 4). The denominator $\overline{f}_{ARC}(\Omega)$ corresponds to the mass fraction of the Arctic irrespective of where air last contacted the PBL.

PBL origin region Ω_i	Free troposphere, $\frac{\overline{f}_{ARC}(\Omega_i)}{\overline{f}_{ARC}(\Omega)}$		Lower troposphere, $\frac{\overline{f}_{ARC}(\Omega_i)}{\overline{f}_{ARC}(\Omega)}$		Middle troposphere, $\frac{\overline{f}_{ARC}(\Omega_i)}{\overline{f}_{ARC}(\Omega)}$	
	DJF	JJA	DJF	JJA	DJF	JJA
ARC	37%	47%	70%	75%	23%	34%
MID	51%	46%	28%	23%	62%	57%
STH	12%	6.5%	1.7%	1.6%	16%	8.6%

free troposphere above 500 mb. The Ω_{STH} airmass fraction increases dramatically upon crossing the tropopause, reflecting the fact that the main pathway that connects the PBL south of 25°N to the Arctic intersects the tropical and subtropical lower stratosphere. More specifically, the monthly evolution of $f(\mathbf{r}, t \,|\, \Omega_{STH})$ (not shown) reveals that Ω_{STH} air is transported into the tropical upper troposphere and lower stratosphere over the SH (NH) subtropics during boreal winter (summer) (i.e., the ascending branches of the Hadley cell). Thereafter, Ω_{STH} air is quasi-isentropically transported the Arctic during boreal summer, coincident with the relaxation of the tropical/extratropical mixing barrier in the lower stratosphere (Chen 1995).

The pathway that connects Ω_{STH} air to the Arctic is broadly consistent with strong evidence from models and observations that significant two-way mass and tracer exchange occurs at the NH subtropical tropopause, where quasi-isentropic mixing around the subtropical jet stream enhances transport between the tropical upper troposphere and extratropical lower stratosphere (e.g., Sprenger and Wernli 2003; Škerlak et al. 2014). Because the focus of this study is on the Arctic free troposphere, however, we reserve further discussion of this transport pathway to future work.

b. Origin over NH midlatitudes

The vertical profiles $\overline{f}^{DJF}_{ARC}(p \,|\, \Omega_i)$ and $\overline{f}^{JJA}_{ARC}(p \,|\, \Omega_i)$ for the Ω_i spanning Ω_{MID} (Fig. 6) reveal large seasonal differences in the regions where Arctic air last contacted the midlatitude PBL. Above 700 mb the Ω_i airmass fractions each vary by as much as about 20%–30% between boreal winter and summer, while seasonal variations below 700 mb are relatively weaker, albeit statistically significant. Note that in Fig. 6 the airmass fractions have first been normalized by $\overline{f}_{ARC}(p \,|\, \Omega_{MID})$ in order to ensure that their sum is 100% at each pressure level.

During winter, most of the air below 700 mb in the Arctic originated over the eastern Pacific and over Europe, with $\overline{f}^{DJF}_{ARC}(p \,|\, \Omega_{EPAC})$ and $\overline{f}^{DJF}_{ARC}(p \,|\, \Omega_{EUR})$ respectively comprising 25% (±1.6%) and 20% (±2.3%) of all midlatitude air in the lower Arctic (Table 2). By comparison, during boreal summer, last contact at the midlatitude PBL occurred primarily over North America [23% (±1.4%)], the Atlantic Ocean [16% (±2.0%)], and Asia [29% (±0.85%)].

Above 700 mb, seasonal variations in the airmass fractions are relatively larger. Midlatitude air is primarily of ocean origin during winter, when the midlatitude storm tracks are strongest and when contours of $\overline{f}^{DJF}(\mathbf{r} \,|\, \Omega_{MID})$ extend isentropically back to the midlatitude eastern Pacific and Atlantic PBL (Fig. 7a). Correspondingly, $\overline{f}^{DJF}_{ARC}(\Omega_{EPAC})$ and $\overline{f}^{DJF}_{ARC}(\Omega_{ATL})$ respectively explain 26% (±1.9%) and 21% (±0.87%) of the 300–700-mb column integrated mass $\overline{f}^{DJF}_{ARC}(\Omega_{MID})$ (Table 2). By comparison, during summer 41% (±1.0%) and 24% (±1.5%) of midlatitude air above 700 mb originated over Asia and North America (Table 2) and contours of $\overline{f}^{JJA}(\mathbf{r} \,|\, \Omega_{ASI})$ and $\overline{f}^{JJA}(\mathbf{r} \,|\, \Omega_{NAM})$ penetrate across isentropes into the midlatitude upper troposphere (Fig. 7b). Interestingly, $\overline{f}^{JJA}(\mathbf{r} \,|\, \Omega_{ASI})$ extends still higher into the lower stratosphere during boreal summer, a signature that persists in the Arctic lower stratosphere into the following winter. This persistence of Asian air is discussed in more detail in the next section, where we interpret the airmass fractions in terms of the large-scale circulation.

5. Large-scale circulation constraints on Arctic airmass origin

To aid in the interpretation of the airmass fractions, we now examine seasonal variations in the large-scale circulation. A discussion of the fidelity of the modeled circulation compared to observations, and implications for our interpretations, is reserved for section 6.

a. Lower Arctic

It has long been appreciated that large-scale stationary waves play a key role in accumulating and transporting pollutants from midlatitudes into the Arctic

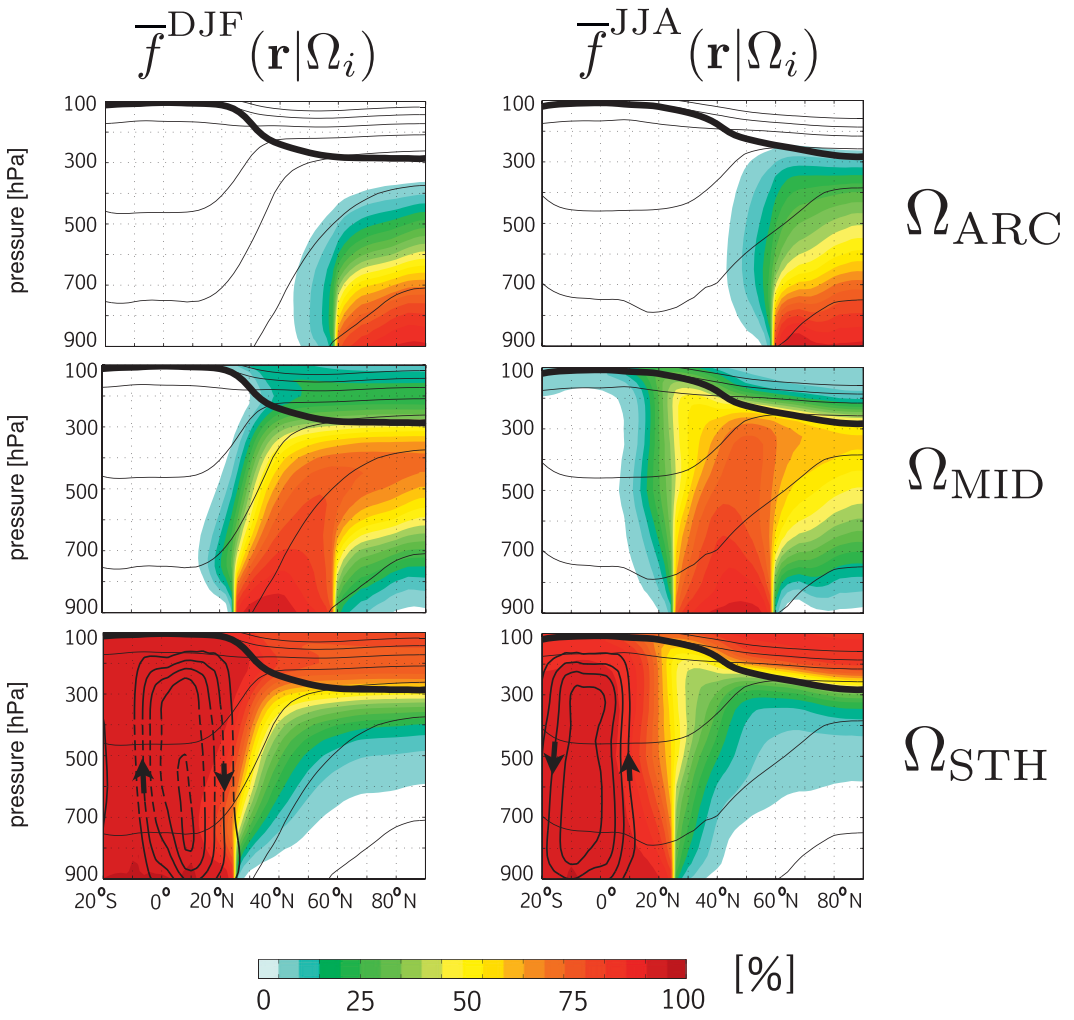

FIG. 5. The fraction of air that last contacted the PBL over (top) Ω_{ARC}, (middle) Ω_{MID}, and (bottom) Ω_{STH}. DJF and JJA climatological mean airmass fractions $\overline{f}^{\mathrm{DJF}}(\mathbf{r}\,|\,\Omega_i)$ and $\overline{f}^{\mathrm{JJA}}(\mathbf{r}\,|\,\Omega_i)$ are shown in the left and right panels, respectively. The zonally averaged seasonal mean thermal tropopause is indicated by the thick black line. Seasonal mean isentropes are overlaid in black [20-K contour interval for isentropes between 270 and 390 K (DJF) and between 290 and 390 K (JJA)]. The mean streamfunction (contour interval: 60×10^9 kg s^{-1}) has also been overlaid on $\overline{f}^{\mathrm{DJF}}(\mathbf{r}\,|\,\Omega_{\mathrm{STH}})$ and $\overline{f}^{\mathrm{JJA}}(\mathbf{r}\,|\,\Omega_{\mathrm{STH}})$ in order to provide a sense for the zonally averaged tropospheric circulation in the tropics and subtropics.

(e.g., Iversen and Joranger 1985; Barrie 1986; Law and Stohl 2007). Correspondingly, large fractions of Ω_{MID} air in the lower troposphere overlie regions where mean cyclonic flow (i.e., low-level convergence) drives Ω_{MID} air out of the boundary layer and into the middle troposphere (Fig. 8). In particular, during winter when strong cyclonic flow prevails over the North Pacific (Aleutian low) and over the North Atlantic (Icelandic low), the largest contributions to $\overline{f}^{\mathrm{DJF}}(\mathbf{r}\,|\,\Omega_{\mathrm{MID}})$ originate over the oceans. Conversely, air that last contacted the PBL over land encounters mean low-level divergence and is rapidly stripped of its Ω_i label over the neighboring PBL.

After escaping the boundary layer, Ω_{MID} air is transported efficiently into the Arctic during winter by strong poleward flow over the North Pacific and over Canada (Raatz and Shaw 1984; Barrie 1986). Whereas these motions ensure that Ω_{EPAC} air is efficiently transported into the Arctic, anticyclonic flow associated with the Azores high draws Ω_{ATL} air southward, where it risks being relabeled at the PBL, resulting in a distribution $\overline{f}^{\mathrm{DJF}}(\mathbf{r}\,|\,\Omega_{\mathrm{ATL}})$ that is relatively weaker at high latitudes than $\overline{f}^{\mathrm{DJF}}(\mathbf{r}\,|\,\Omega_{\mathrm{EPAC}})$ (Fig. 7a). A similar southward transport pattern over the Atlantic has been observed in the distributions of pollutants emitted over Europe (Duncan and Bey 2004).

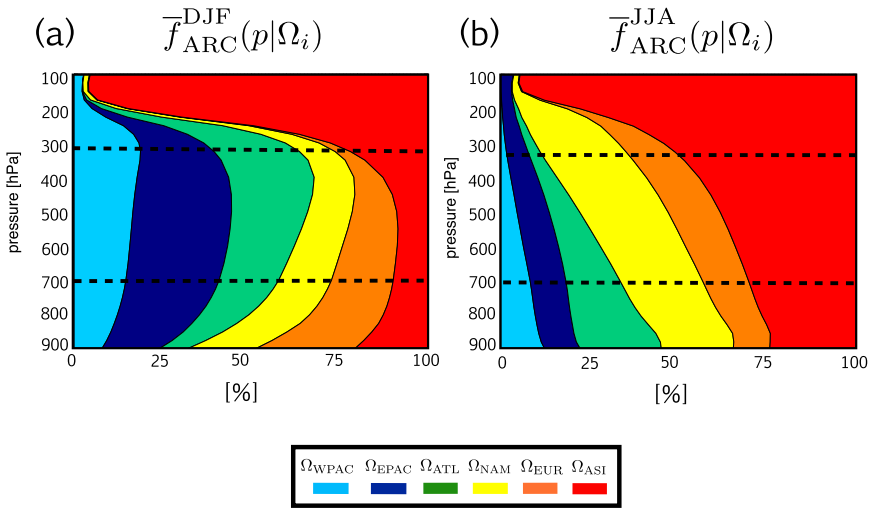

FIG. 6. (a) Vertical profiles of the DJF climatological mean airmass fractions in the Arctic that last contacted the PBL over the WPAC, EPAC, ATL, NAM, EUR, and ASI origin regions. Airmass fractions have been averaged over latitudes poleward of 60°N and normalized by the Arctic fraction that last had PBL contact over NH midlatitudes $\overline{f}^{\mathrm{DJF}}_{\mathrm{ARC}}(p\,|\,\Omega_{\mathrm{MID}})$, which during winter accounts for 51% (±2.2%) of the Arctic free troposphere (i.e., the 300–900-mb column integrated mass $\overline{f}^{\mathrm{DJF}}(\Omega)$; Table 1). (b) As in (a), but for JJA. The midlatitude airmass fraction in the normalization $\overline{f}^{\mathrm{JJA}}_{\mathrm{ARC}}(\Omega_{\mathrm{MID}})$ contributes 46% (±1.1%) of the total mass of the Arctic free troposphere during summer (Table 1).

By comparison, during boreal summer mean anticyclonic motions over the oceans ensure that air that is labeled over Ω_{EPAC}, Ω_{WPAC}, and Ω_{ATL} diverges outward at the surface over Europe and North America, where its Ω_i label is stripped upon recontact with the boundary layer (not shown). Meanwhile, Ω_{MID} air that originates over land is driven away from the boundary layer, consistent with mean low-level convergence and ascent over North America and Asia, although low-level poleward motions over midlatitudes are relatively weaker in summer compared to winter. Hence, overall, there is less air of midlatitude origin in the lower Arctic during summer (i.e., ~5%; Table 1).

Seasonal changes in the thermal structure of the Arctic may also explain why there is less air of midlatitude origin in the Arctic during summer. At 800 mb large values of $\overline{f}^{\mathrm{JJA}}(\mathbf{r}\,|\,\Omega_{\mathrm{ARC}})$ are collocated with convective clouds (Fig. 9a), consistent with warmer temperatures and weaker thermal stratification that enhance the vertical mixing of Ω_{ARC} air away from the Arctic surface. Hence, the confluence of both weaker poleward motions over midlatitudes and enhanced vertical mixing near the Arctic surface reduce the amount of midlatitude boundary layer air in the Arctic during boreal summer.

Finally, it is worth briefly commenting on the strong vertical gradients in $\overline{f}^{\mathrm{DJF}}(\mathbf{r}\,|\,\Omega_{\mathrm{ATL}})$ at 60°N that seem to

TABLE 2. The DJF and JJA climatological mean fraction of the Arctic that last contacted the midlatitude PBL over the western Pacific, the eastern Pacific, the Atlantic, North America, Europe, and Asia. Airmass fractions corresponding to the Ω_i origin regions have been averaged over latitudes poleward of 60°N and column integrated over the free troposphere (300–900 mb; column 2), the lower troposphere (700–900 mb; column 3), and the middle-to-upper troposphere (300–700 mb; column 4). The denominators $\overline{f}^{\mathrm{DJF}}_{\mathrm{ARC}}(\Omega_{\mathrm{MID}})$ and $\overline{f}^{\mathrm{JJA}}_{\mathrm{ARC}}(\Omega_{\mathrm{MID}})$ correspond to the DJF and JJA climatological mean fraction of the Arctic that last contacted the PBL over NH midlatitudes.

	Free troposphere, $\frac{\overline{f}_{\mathrm{ARC}}(\Omega_i)}{\overline{f}_{\mathrm{ARC}}(\Omega_{\mathrm{MID}})}$		Lower troposphere, $\frac{\overline{f}_{\mathrm{ARC}}(\Omega_i)}{\overline{f}_{\mathrm{ARC}}(\Omega_{\mathrm{MID}})}$		Middle troposphere, $\frac{\overline{f}_{\mathrm{ARC}}(\Omega_i)}{\overline{f}_{\mathrm{ARC}}(\Omega_{\mathrm{MID}})}$	
PBL origin region Ω_i	DJF	JJA	DJF	JJA	DJF	JJA
WPAC	16%	9.1%	13%	10%	16%	9.0%
EPAC	26%	6.2%	25%	9.8%	26%	5.7%
ATL	20%	9.0%	15%	16%	21%	8.0%
NAM	13%	24%	16%	23%	12%	24%
EUR	13%	12%	20%	13%	12%	13%
ASI	12%	40%	12%	29%	12%	41%

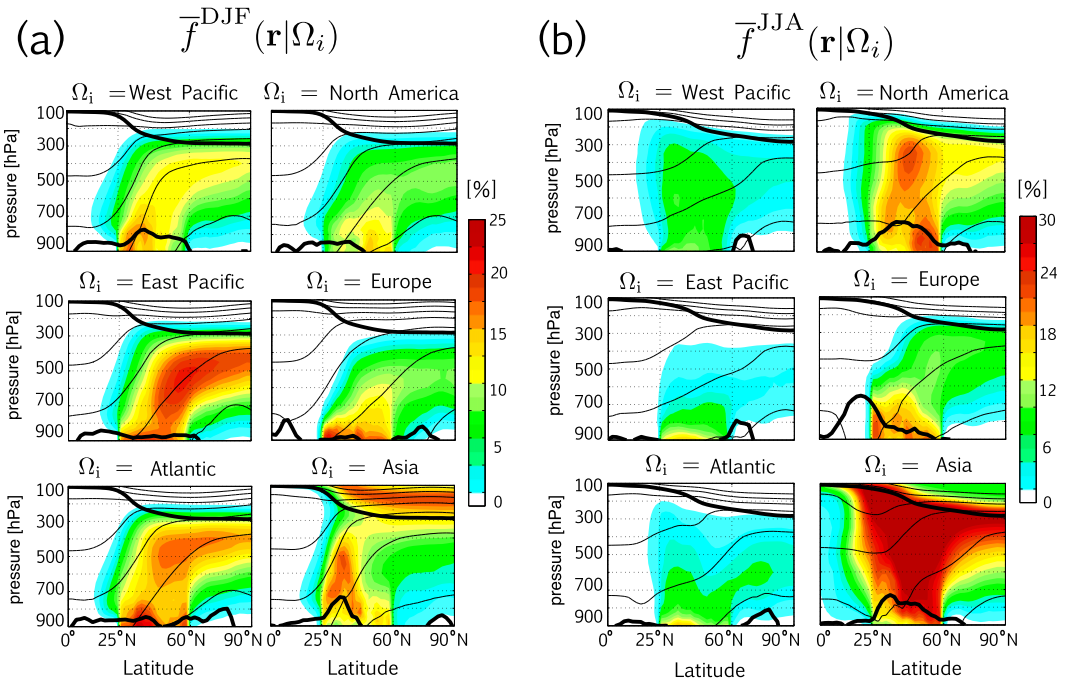

FIG. 7. (a) The DJF climatological mean airmass fractions $\overline{f}^{\mathrm{DJF}}(\mathbf{r}\,|\,\Omega_i)$, corresponding to air that last contacted the PBL over the land and ocean origin regions spanning NH midlatitudes. The zonally averaged DJF mean thermal tropopause is indicated by the top thick black line; the bottom black line denotes the DJF mean planetary boundary layer, averaged over longitudes spanning Ω_i. Wintertime mean isentropes have also been averaged over longitudes in Ω_i and are overlaid in the thin black contours (contour interval: 20 K). (b) As in (a), but for JJA. Note the different color bar.

indicate the presence of a transport barrier over the North Atlantic during boreal winter (Fig. 7a). Further examination of $\overline{f}^{\mathrm{DJF}}(\mathbf{r}\,|\,\Omega_{\mathrm{ATL}})$ at 60°N (Fig. 9b, left) reveals that the strongest gradients are concentrated to the southeast of Greenland, where there are large convective cloud fractions and an elevated PBL (Fig. 2b; see also Fig. A1). Both high clouds and an elevated PBL are consistent with enhanced turbulent mixing by strong surface winds in that region that stem from the deformation of the Atlantic jet by topography over Greenland (Moore and Renfrew 2005; Sampe and Xie 2007). Correspondingly, strong surface winds tend to enhance the turbulent mixing of Ω_{ARC} air away from the ocean surface as well as the rate with which Ω_{ATL} air is relabeled at the PBL upon entering the Arctic.

It is also possible that strong vertical gradients in $\overline{f}^{\mathrm{DJF}}(\mathbf{r}\,|\,\Omega_{\mathrm{ATL}})$ are partly maintained by diabatic heating within the Atlantic storm track, consistent with previous studies that have linked the cross-isentropic ascent of midlatitude pollutants at high latitudes to heating within warm conveyer belts (Klonecki et al. 2003; Sinclair et al. 2008; Madonna et al. 2014). Whereas this heating helps to maintain strong vertical gradients in $\overline{f}^{\mathrm{DJF}}(\mathbf{r}\,|\,\Omega_{\mathrm{ATL}})$ that persist well above the PBL, weak gradients in $\overline{f}^{\mathrm{DJF}}(\mathbf{r}\,|\,\Omega_{\mathrm{EUR}})$ (Fig. 9b, right), by comparison, reflect cooling over the Eurasian snow and ice pack as Ω_{EUR} air is relabeled at the PBL (Barrie 1986).

b. *Middle Arctic*

In the middle and upper Arctic, where interactions with the boundary layer are considerably weaker, it is instructive to recast the tracer Eq. (1) in terms of the residual mean circulation as in Andrews et al. (1987). We assume that the influence of boundary condition [Eq. (2)] is relatively weak so that a comparison of the terms (i) $\overline{\partial v' f'(\Omega_i)/\partial y}$ and (ii) $\overline{v^* \partial f(\Omega_i)/\partial y}$ provides a sense for the relative roles that meridional transient eddies and advection by the residual mean circulation play in transporting Ω_{MID} air into the middle and upper Arctic. (Asterisks and primes denote deviations from zonal and time means, respectively; transient eddies have been calculated using daily mean data.)

During winter the climatological mean variance of the eddy meridional velocity $\overline{v'v'}^{\mathrm{DJF}}$ is strongly coupled to the midlatitude tropospheric jet (Fig. A2). Transient eddies maximize over the northwest coast of North America and over the western and central Atlantic basin, coincident with the outflow regions of warm conveyer belts (Eckhardt et al. 2004; Sinclair et al. 2008; Madonna et al. 2014). Correspondingly, we find that the

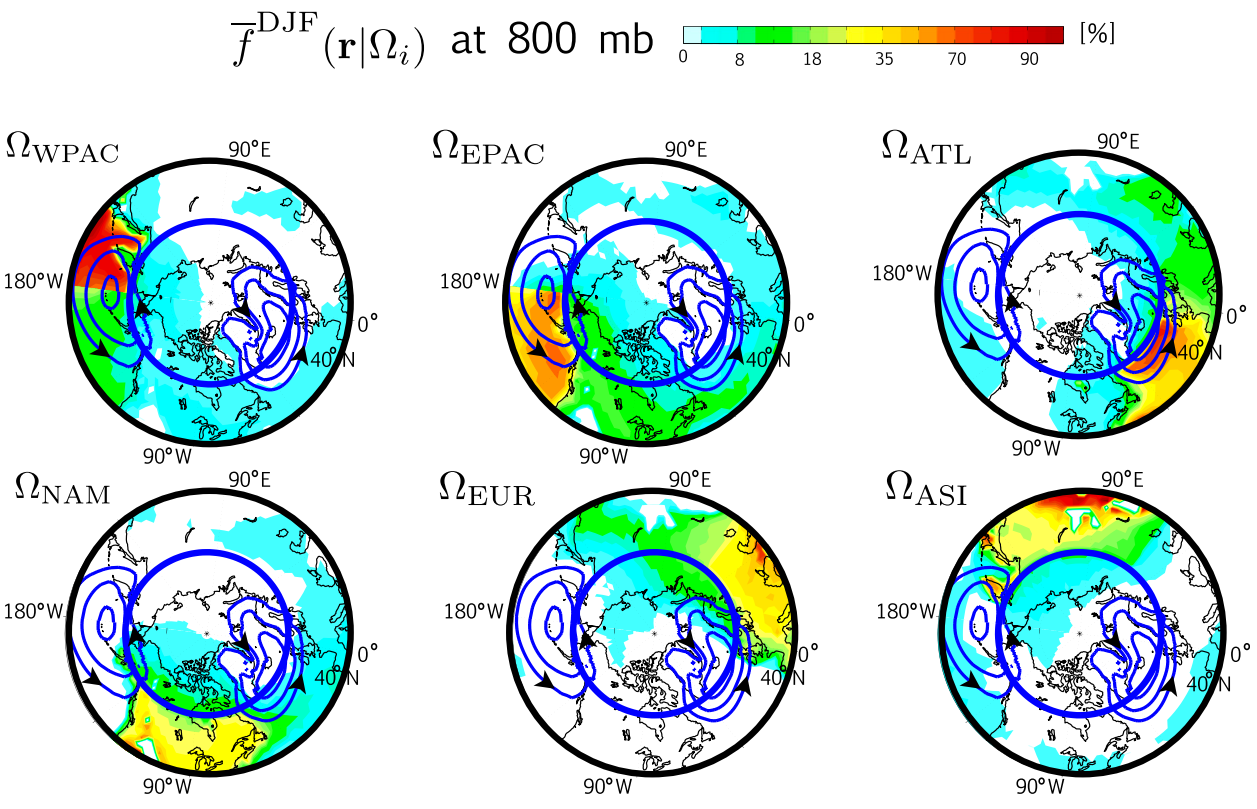

FIG. 8. The DJF climatological mean fraction of air at 800 mb that last contacted the midlatitude PBL over (top) the western Pacific, the eastern Pacific, and the Atlantic and (bottom) North America, Europe, and Asia, overlaid by the DJF mean sea level pressure (contours are shown for pressures between 980 and 996 mb; contour interval is 4 mb). Note that a nonlinear color bar has been used in order to highlight the spatial patterns of the Ω_i airmass fractions over the Arctic. In addition, recall that the sum of the six $\overline{f}^{\mathrm{DJF}}(\mathbf{r}\,|\,\Omega_i)$ is $\overline{f}^{\mathrm{DJF}}(\mathbf{r}\,|\,\Omega_{\mathrm{MID}})$. The thick blue circle denotes the equatorward edge of Ω_{ARC} at 60°N.

eddy-induced transport of Ω_{EPAC} air is much larger than transport by the residual mean meridional velocity, with term (i) exceeding (ii) by, at places, a factor of 2 (Fig. 10a). Vertical profiles of (i) and (ii), averaged over 25°–60°N and evaluated for the Ω_{WPAC} and Ω_{ATL} airmass fractions, reveal that transport by transient eddies also dominates the poleward transport of western Pacific and Atlantic boundary layer air (Fig. 10b).

During summer, by comparison, $\overline{v'v'}$ decreases significantly (not shown), coincident with a reduced frequency of warm conveyer belts (Eckhardt et al. 2004) as well as decreases in other eddy statistics over midlatitudes, including heat and momentum fluxes as documented in Wu et al. (2011). Rather, the distribution of $\overline{f}^{\mathrm{JJA}}(\mathbf{r}\,|\,\Omega_{\mathrm{MID}})$ is more consistent with boundary layer ventilation via large-scale convection associated with the North American and Asian monsoons.

In particular, $\overline{f}^{\mathrm{JJA}}(\mathbf{r}\,|\,\Omega_{\mathrm{NAM}})$ evaluated at 300 mb (Fig. 11) reveals large fractions of Ω_{NAM} air over the southwest coast of North America that spread eastward over the Atlantic with the midlatitude jet. Similarly, the 300-mb distribution of $\overline{f}^{\mathrm{JJA}}(\mathbf{r}\,|\,\Omega_{\mathrm{ASI}})$ reveals that Ω_{ASI} air is confined within the Asian monsoon anticyclone and drawn eastward over the Pacific and into the Arctic by the mean westerly flow. Moreover, the upper-level divergent flow in summer, quantified in terms of the 300-mb eddy geopotential height $\overline{\Phi^*}^{\mathrm{JJA}}$, reveals strong mean equatorward motions over Canada and North America that deflect recently labeled Ω_{NAM} air away from the Arctic, enhancing its likelihood of being relabeled at the PBL. By comparison, Ω_{ASI} air north of the subtropical anticyclone travels eastward at the northern edge of Ω_{ASI} where, coincident with strong longitudinal gradients in $\overline{\Phi^*}^{\mathrm{JJA}}$, air is efficiently transported poleward over Siberia.

Finally, we comment on the large fractions of Ω_{ASI} air that span the Arctic lower stratosphere during winter (previously mentioned in section 4b). The monthly evolution of $f(\mathbf{r},\, t\,|\,\Omega_{\mathrm{ASI}})$ (Fig. 12) reveals that large fractions of Ω_{ASI} air in winter stem from transport that occurred during the previous summer monsoon. Between April and August Ω_{ASI} air is lofted out of the PBL into the extratropical upper troposphere and lower stratosphere, followed by quasi-horizontal transport to

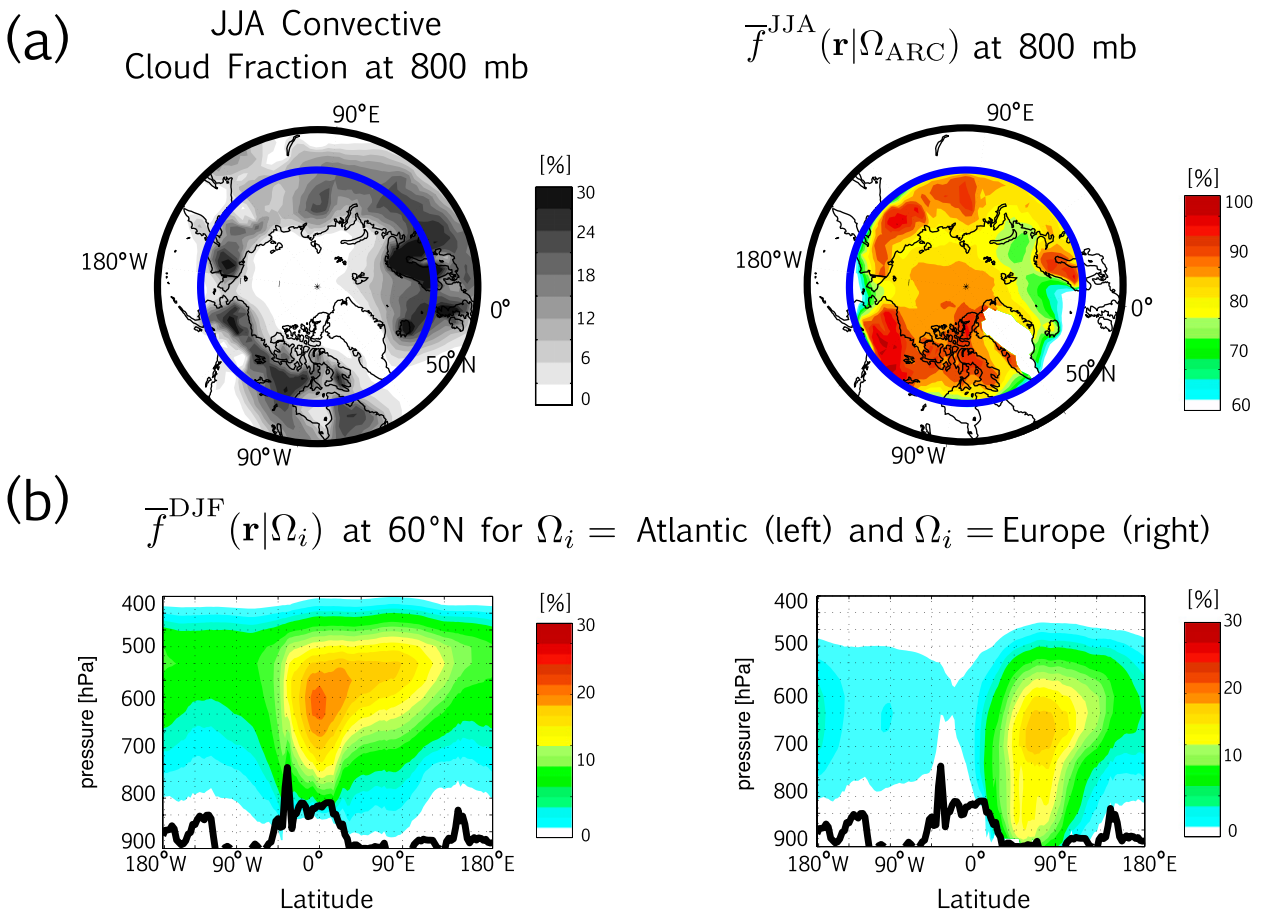

FIG. 9. (a) The JJA climatological mean (left) convective cloud fraction evaluated at 800 mb and (right) airmass fraction at 800 mb that last had PBL contact at Ω_{ARC}. The thick blue circle denotes the equatorward edge of Ω_{ARC} at 60°N. (b) Cross sections of the DJF climatological mean airmass fraction (left) $\overline{f}^{\mathrm{DJF}}(\mathbf{r}\,|\,\Omega_{\mathrm{ATL}})$ and (right) $\overline{f}^{\mathrm{DJF}}(\mathbf{r}\,|\,\Omega_{\mathrm{EUR}})$ at 60°N. The thick black line denotes the DJF climatological mean PBL, also evaluated at 60°N.

NH high latitudes during fall, where it lingers until the end of winter. By comparison, monthly profiles for the other midlatitude airmass fractions do not reveal any significant transport within the lower stratosphere (not shown).

The transport of Ω_{ASI} air into the lower stratosphere is consistent with growing evidence that the Asian summer monsoon plays a key role in the troposphere-to-stratosphere transport of pollutants emitted over midlatitudes (Rosenlof et al. 1997; Park et al. 2004; Li et al. 2005; Randel and Park 2006). The horizontal structure of $\overline{f}^{\mathrm{JJA}}(\mathbf{r}\,|\,\Omega_{\mathrm{ASI}})$ in the lower troposphere (not shown) reveals that Ω_{ASI} air is transported upward primarily over the Tibetan Plateau and organized aloft within the monsoon anticyclone, consistent with Bergman et al. (2013) and Škerlak et al. (2014). A detailed look at this transport pathway, however, is beyond the scope of this study and will be examined in future work.

6. Discussion

The air masses defined and computed here quantify transport in a tracer-independent manner and provide an easily computed model metric for assessing tropospheric transport in the Arctic. Unlike the usual basic flow diagnostics (mean winds, streamfunctions, and mean eddy diffusivities) airmass fractions represent the integrated effects of advection and diffusion and their interactions with the PBL. Although the airmass fractions can be interpreted, as we have done here, in terms of basic circulation diagnostics, we stress that we could not have deduced the patterns and seasonalities of the airmass fractions, let alone their quantitative magnitudes, without explicitly computing them.

When interpreting airmass fractions one must keep their physical definitions firmly in mind. By construction, the air masses defined here track air since last PBL contact. Therefore, transport pathways within the PBL

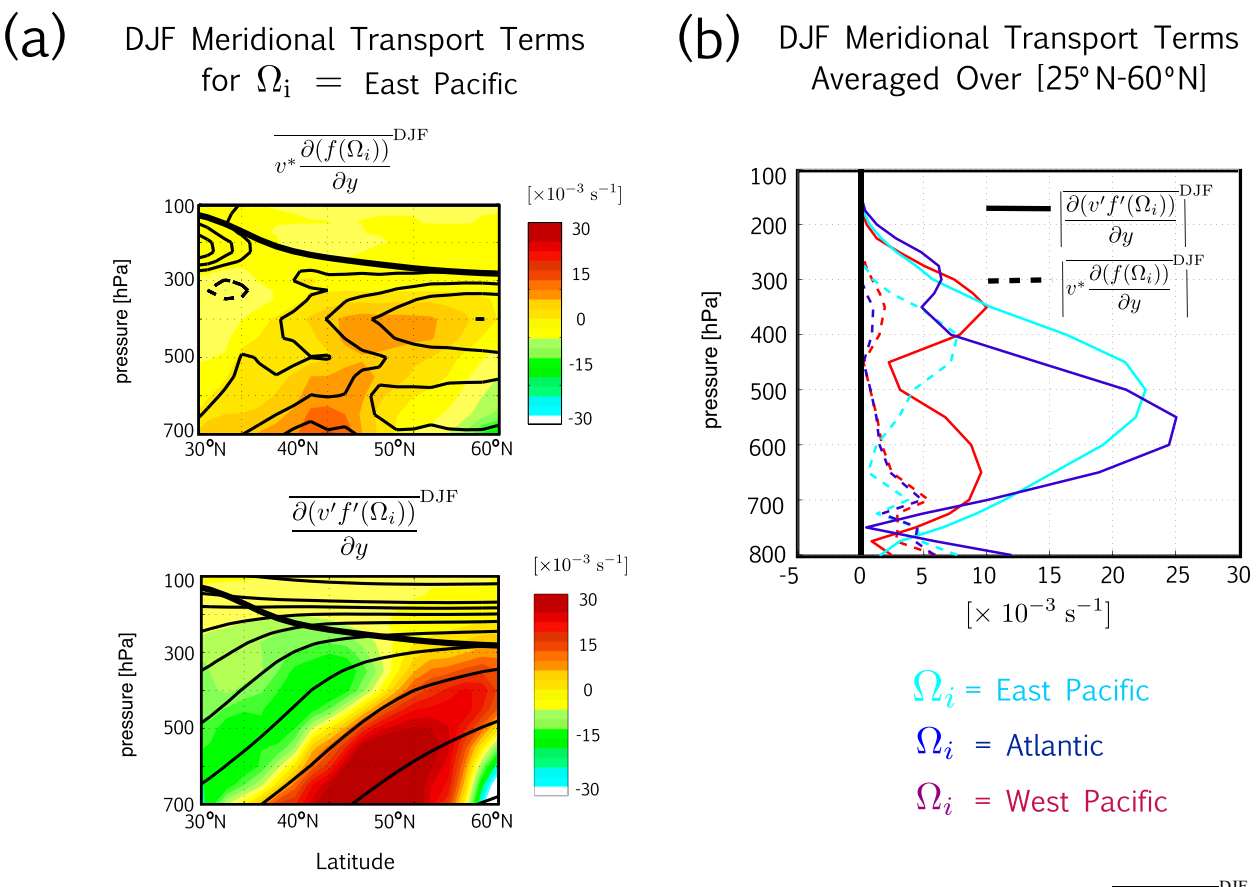

FIG. 10. (a) Comparison of the DJF climatological mean meridional advective- and eddy-induced transport terms (top) $\overline{v^* \partial f(\Omega_i)/\partial y}^{\mathrm{DJF}}$ and (bottom) $\overline{\partial v' f'(\Omega_i)/\partial y}^{\mathrm{DJF}}$ for air that last contacted the PBL over the eastern Pacific. The DJF residual mean meridional velocity $\overline{v^*}^{\mathrm{DJF}}$ is overlaid on the top panel with the black contours (contour interval: 0.3 m s^{-1}). DJF climatological mean isentropes are overlaid on the bottom panel with the black contours (contour interval: 10 K). The DJF mean thermal tropopause is indicated in both panels by the thick black line. (b) Comparison of the advective and eddy transport terms (dashed and solid lines respectively) for the airmass fractions that last contacted the PBL over the eastern Pacific (cyan), the Atlantic (blue), and the western Pacific (red). The transport terms have been averaged over the midlatitude origin region (i.e., latitudes 25°–60°N) and have been expressed in terms of their absolute magnitudes.

are not captured by our diagnostics as Ω_i air is stripped of its label when it recontacts the boundary layer. Nonetheless, the boundary conditions not only ensure that f may be interpreted as a fraction, but also recognize that many trace species lose their characteristic chemical signatures in the PBL through processes such as turbulent mixing and scavenging, rendering airmass origin with respect to the PBL a particularly meaningful transport measure.

Before concluding we briefly discuss possible implications that biases in the modeled large-scale circulation may have on our interpretations. We begin with the position of the midlatitude tropospheric jet, which, as in other GCMs run at similar horizontal resolutions, is too far equatorward and poleward in winter and summer, respectively (Molod et al. 2012). The fact that jet biases are largest over the Atlantic Ocean may impact our conclusion regarding the relative importance of the Ω_{EPAC} and Ω_{ATL} origin regions in supplying boundary layer air to the Arctic during winter. While we can speculate that an equatorward bias in the Atlantic jet may lead to an underestimate in the magnitude of $\overline{f}^{\mathrm{DJF}}(\mathbf{r} \mid \Omega_{\mathrm{ATL}})$ (i.e., the jet is shifted off the Ω_{ATL} origin region compared to its observed position), a quantitative understanding for how sensitive airmass origin is to jet location and strength can only be determined by explicitly calculating the airmass fractions. This investigation is beyond the scope of this study and will be pursued in future work.

Another issue is the fidelity of the model's representation of convective transport. Convective transport realized by the large-scale flow will reflect model biases in, for example, the location and strength of the Asian monsoon. Indeed, a comparison of the model's JJA climatological mean velocity potential at 200 mb with MERRA reanalysis indicates that that the monsoon is approximately 10° too far east, a bias that is also present

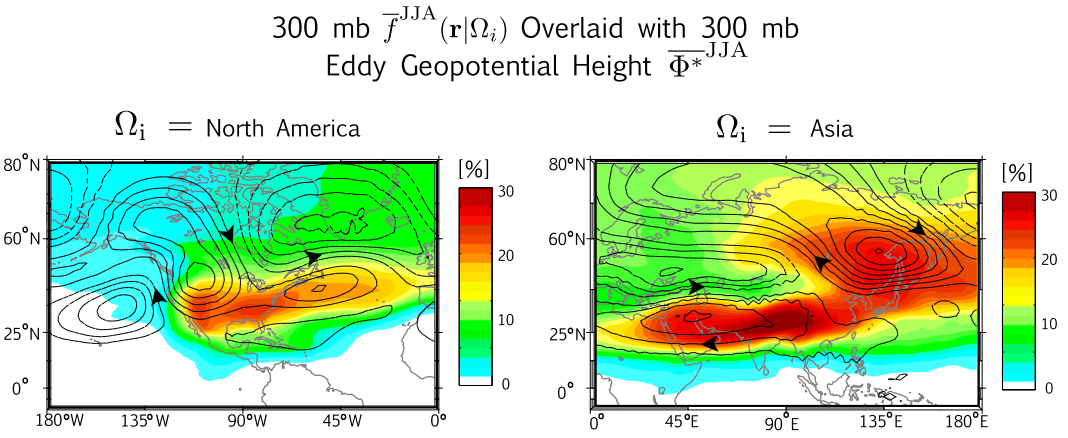

FIG. 11. The climatological mean airmass fraction corresponding to last PBL contact over (left) North America and (right) Asia, evaluated at 300 mb during NH summer. The thin black contours show the JJA climatological mean eddy geopotential height $\overline{\Phi^*}^{JJA}$ which provides a sense for the upper tropospheric divergent circulation (contour interval: 24 m).

in other atmosphere GCMs (Neale et al. 2010; Molod et al. 2012). If anything, however, this bias implies that our results underestimate the overwhelmingly large amount of Ω_{ASI} air in the Arctic during boreal summer and our main conclusions are unchanged.

Subgrid-scale transport will also reflect additional uncertainties in the model's parameterized convection. However, as shown in Ott et al. (2011), ensembles of integrations using GEOS-5 reveal that carbon monoxide (CO) profiles are only weakly sensitive to perturbations in the convective mass flux and moist physics parameters that inform the model's relaxed Arakawa–Schubert convection scheme. In particular, global sensitivities in modeled CO distributions are found to be only 3%, or less than the model internal variability. Hence, we do not expect that uncertainties in unresolved convective transport will significantly change our conclusions.

Finally, one possible concern is that the modeled PBL is biased high during boreal summer because it fails to properly collapse (i.e., cool) at night (McGrath-Spangler and Molod 2014). This bias notwithstanding, however, McGrath-Spangler and Molod (2014) show that transport sensitivities to PBL definition in GEOS-5 are large only on daily and instantaneous time scales and become negligible on the seasonal and annual time scales of interest in the present study. Hence, we do not worry that our results hinge on the particularities of the modeled PBL.

7. Conclusions

Uncertainties in trace species distributions in the Arctic stem partly from the lack of available diagnostics that quantify the underlying advective–diffusive transport, independent of their emissions and/or chemistry. Here, we have used airmass fractions to identify the regions where Arctic air last had contact with the PBL. Specifically, the mixing ratio $f(\mathbf{r}, t \,|\, \Omega_i)$ quantifies the admixture of air with Ω_i and Ω_i^c labels (ones and zeros, respectively), which allows us to interpret f as the desired mass fraction. Origin regions in the PBL have been defined with a focus on assessing where Arctic air last contacted the midlatitude PBL and have been calculated for a comprehensively modeled flow (GEOSCCM) forced under GHG and ODS scenarios representative of the "current" climate. Annual and seasonal mean climatologies reveal the following:

1) For all seasons, the lower Arctic is dominated by air that last contacted the PBL poleward of 60°N. By comparison, the air above 700 mb is primarily of midlatitude origin, although a relatively smaller but significant fraction last contacts the PBL south of 25°N (~12%). Seasonal variations in the airmass fractions are largest above 700 mb, where there is less air of midlatitude origin during boreal summer compared to winter.
2) There are large seasonal differences in the midlatitude regions where Arctic air last contacted the PBL. During winter, the air above 700 mb originates primarily over the oceans, with 26% (±1.9%) and 21% (±0.87%) of midlatitude air last having contacted the PBL over the eastern Pacific and the Atlantic respectively. By comparison, during summer air is primarily of Asian [41% (±1.0%)] and North American [24% (±1.5%)] origin. Seasonal variations in the lower Arctic are smaller, albeit statistically significant.
3) Seasonal variations in the airmass fractions below 700 mb are interpreted largely in terms of changes in large-scale stationary waves over midlatitudes.

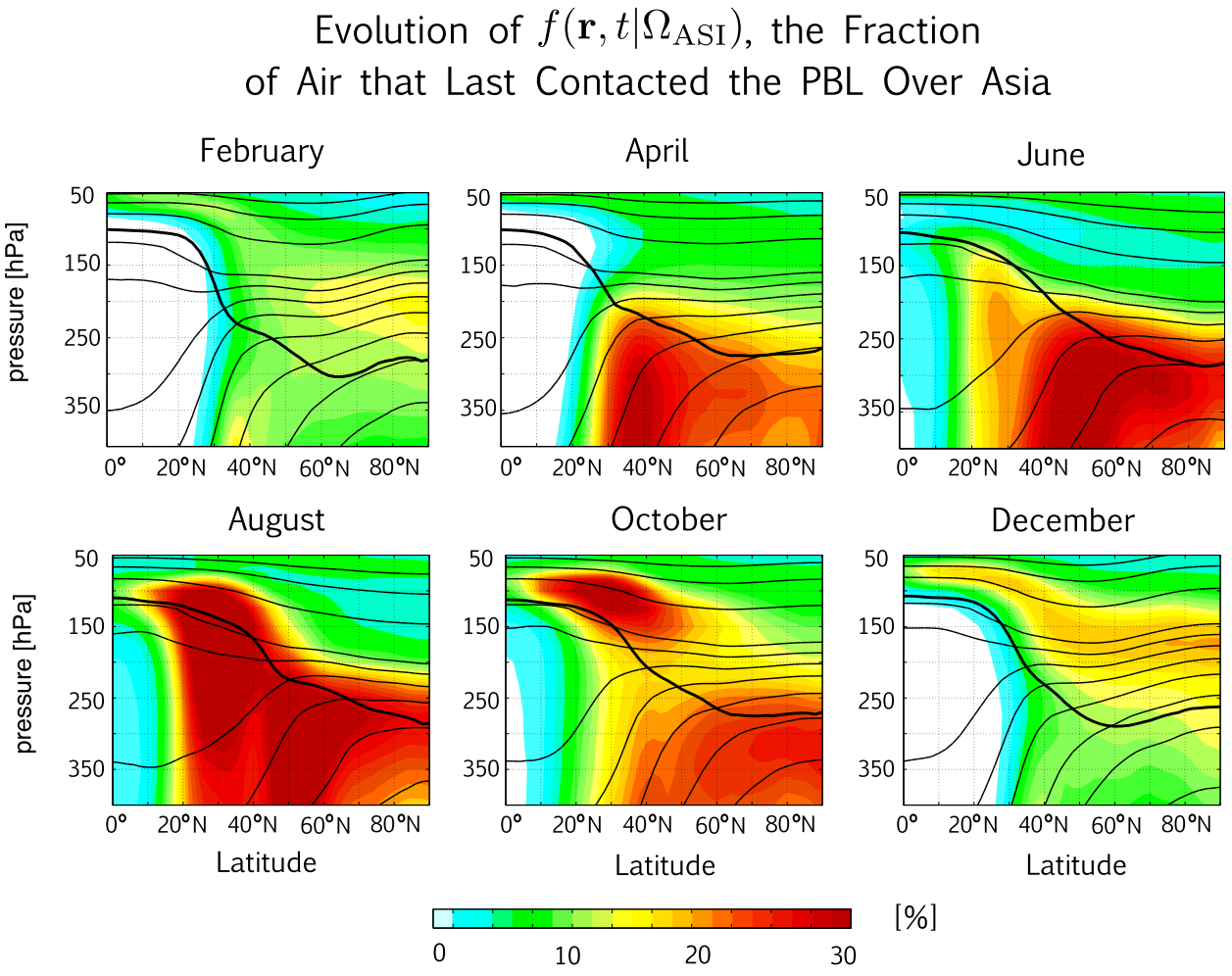

FIG. 12. The monthly evolution of $f(\mathbf{r}, t \mid \Omega_{\mathrm{ASI}})$, the airmass fraction that last contacted the PBL over Asia, shown for a model year after tracers have reached equilibrium. Monthly mean isentropes [contour interval: 10 K (40 K) for isentropes less than (greater than) 360 K] and the monthly mean thermal tropopause are overlaid in the thin and thick black lines, respectively. Note that the vertical axis extends from 50 to 400 mb in order to highlight the extension of Ω_{ASI} air into the lower stratosphere that occurs during NH summer and fall and is associated with the Asian summer monsoon.

During winter, mean cyclonic flow over the oceans and strong poleward motions over the west coast of North America transport Ω_{EPAC} air efficiently out of the boundary layer and into the Arctic. By comparison, during summer anticyclonic flow prevails over the oceans. When coupled with reduced stability in the lower Arctic that enhances the vertical mixing of Ω_{ARC} air away from the boundary layer, this leads to an overall reduction in the amount of midlatitude air in the middle and upper Arctic.

4) Seasonal variations in the airmass fractions above 700 mb largely reflect changes in the large-scale ventilation of Ω_{MID} air out of the boundary layer. During winter, Ω_{MID} air is vigorously transported along isentropes out of the oceans by extratropical cyclones; by comparison, during summer, as the storm tracks weaken over the oceans, midlatitude air is preferentially transported across isentropes over land via large-scale convection.

Throughout, our focus has been exclusively on transport. A natural extension of this study will be to assess how the airmass fractions are modified when information about chemistry and/or emissions is included to better approximate Arctic species with tropospheric lifetimes spanning a few days (e.g., black carbon) to several months (e.g., CO). One way to address this invokes the relationship, not needed for the purposes of this paper, that mass fractions are also equal to the transit-time integrated boundary propagator for mixing ratios specified on Ω (Haine and Hall 2002; Holzer and

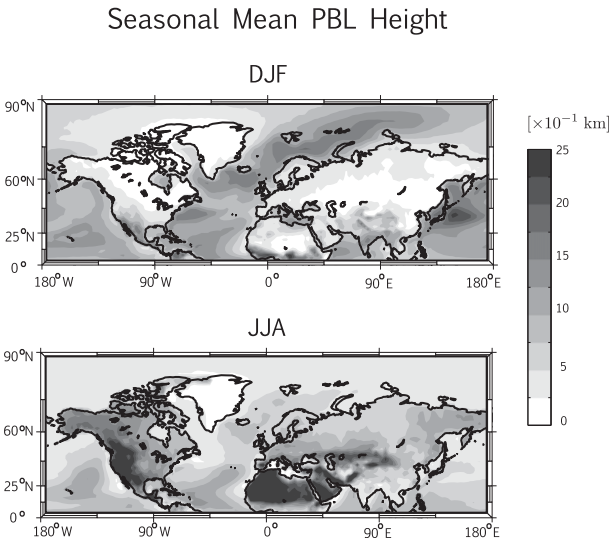

FIG. A1. The climatological mean planetary boundary layer (PBL) height for (top) DJF and (bottom) JJA. The model PBL is calculated online as the height of the lowest model layer in which the eddy diffusion coefficient of heat falls below 2 $m^2 s^{-1}$.

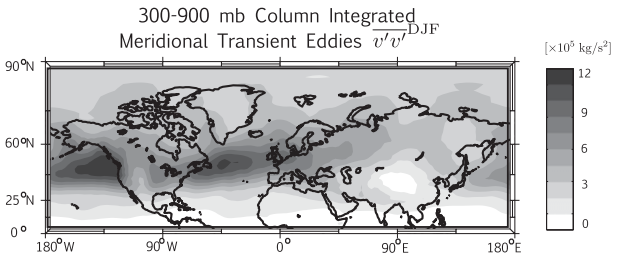

FIG. A2. The DJF climatological mean variance of the eddy meridional velocity $\overline{v'v'}^{DJF}$ column integrated over 300–900 mb. Primes denote deviations from the time mean and have been calculated using daily mean data.

Acknowledgments. This research was supported by an appointment to the NASA Postdoctoral Program at the Goddard Space Flight Center, administered by Oak Ridge Associated Universities through a contract with NASA. The authors also acknowledge support from ARC Grant DP120100674 (M.H.) and NSF Grants AGS-1403676 (D.W.) and AGS-1402931 (M.H. and L.M.P.).

Primeau 2010). To approximate real tracers, the boundary propagator may be calculated for the different regions Ω_i, weighted with decay functions that approximate idealized chemistry and/or deposition and then integrated over the range of transit times since last PBL contact to yield the fraction of the Arctic that originates over Ω_i, subject to the effects of idealized physics and chemistry.

Another important implication of the relationship between f and the boundary propagator is that airmass fractions may not only be computed with transport models, as done here, but they can also be estimated from observable tracer data. This has already been demonstrated for the oceans using simple mixing matrix (e.g., Tomczak 1981) as well as maximum-entropy approaches (Holzer et al. 2010; Khatiwala et al. 2009, 2012). Extending these inversion techniques to estimate boundary layer airmass origin for the Arctic is left for future research.

By interpreting airmass origin in terms of the large scale circulation we have set the stage for examining how airmass origin in the Arctic will respond to future warming. Specifically, how will projected shifts in the tropospheric midlatitude jets and weakened large-scale convection in the extratropics change the regions where Arctic air last encounters the boundary layer? This will be addressed in the second part of this study to be published later, where we assess the climate-change response of airmass origin in the Arctic using an integration of GEOSCCM subject to A1B GHG warming.

APPENDIX

Supporting Figures: Modeled Planetary Boundary Layer Height and Mean Variance of the Eddy Meridional Velocity

Seasonal changes in PBL height (Fig. A1) reveal an elevated (reduced) PBL over land (ocean) during boreal summer. Gross differences between land and ocean, as well as wintertime PBL minima over Canada and summertime maxima over the western United States, are consistent with PBL estimates derived from radiosonde observations (McGrath-Spangler and Molod 2014).

The modeled boreal winter variance of the eddy meridional velocity (Fig. A2) is strongly coupled to the midlatitude tropospheric jet. Transient eddies maximize over the northwest coast of North America and over the western and central Atlantic basin, coincident with the outflow regions of warm conveyer belts (Eckhardt et al. 2004; Sinclair et al. 2008; Madonna et al. 2014).

REFERENCES

Andrews, D., J. Holton, and C. Leovy, 1987: *Middle Atmosphere Dynamics.* Academic Press, 489 pp.

Arakawa, A., and W. H. Schubert, 1974: Interaction of a cumulus cloud ensemble with the large-scale environment, Part I. *J. Atmos. Sci.,* **31,** 674–701, doi:10.1175/1520-0469(1974)031<0674:IOACCE>2.0.CO;2.

Atlas, E. L., B. A. Ridley, and C. A. Cantrell, 2003: The Tropospheric Ozone Production about the Spring Equinox

(TOPSE) experiment: Introduction. *J. Geophys. Res.,* **108,** 8353, doi:10.1029/2002JD003172.

Barnes, E. A., and L. Polvani, 2013: Response of the midlatitude jets, and of their variability, to increased greenhouse gases in the CMIP5 models. *J. Climate,* **26,** 7117–7135, doi:10.1175/JCLI-D-12-00536.1.

Barrie, L. A., 1986: Arctic air pollution: An overview of current knowledge. *Atmos. Environ.,* **20,** 643–663.

Bengtsson, L., K. I. Hodges, and E. Roeckner, 2006: Storm tracks and climate change. *J. Climate,* **19,** 3518–3543, doi:10.1175/JCLI3815.1.

——, ——, and N. Keenlyside, 2009: Will extratropical storms intensify in a warmer climate? *J. Climate,* **22,** 2276–2301, doi:10.1175/2008JCLI2678.1.

Bergman, J. W., F. Fierli, E. J. Jensen, S. Honomichl, and L. L. Pan, 2013: Boundary layer sources for the Asian anticyclone: Regional contributions to a vertical conduit. *J. Geophys. Res. Atmos.,* **118,** 2560–2575, doi:10.1002/jgrd.50142.

Catto, J. L., L. C. Shaffrey, and K. I. Hodges, 2011: Northern Hemisphere extratropical cyclones in a warming climate in the HiGEM high-resolution climate model. *J. Climate,* **24,** 5336–5352, doi:10.1175/2011JCLI4181.1.

Chang, E. K., Y. Guo, and X. Xia, 2012: CMIP5 multimodel ensemble projection of storm track change under global warming. *J. Geophys. Res.,* **117,** D23118, doi:10.1029/2012JD018578.

Chen, P., 1995: Isentropic cross-tropopause mass exchange in the extratropics. *J. Geophys. Res.,* **100** (D8), 16 661–16 673, doi:10.1029/95JD01264.

Delcambre, S. C., D. J. Lorenz, D. J. Vimont, and J. E. Martin, 2013: Diagnosing Northern Hemisphere jet portrayal in 17 CMIP3 global climate models: Twentieth-century intermodel variability. *J. Climate,* **26,** 4910–4929, doi:10.1175/JCLI-D-12-00337.1.

Douglass, A. R., C. J. Weaver, R. B. Rood, and L. Coy, 1996: A three-dimensional simulation of the ozone annual cycle using winds from a data assimilation system. *J. Geophys. Res.,* **101** (D1), 1463–1474, doi:10.1029/95JD02601.

Duncan, B., and I. Bey, 2004: A modeling study of the export pathways of pollution from Europe: Seasonal and interannual variations (1987–1997). *J. Geophys. Res.,* **109,** D08301, doi:10.1029/2003JD004079.

Eckhardt, S., A. Stohl, H. Wernli, P. James, C. Forster, and N. Spichtinger, 2004: A 15-year climatology of warm conveyor belts. *J. Climate,* **17,** 218–237, doi:10.1175/1520-0442(2004)017<0218:AYCOWC>2.0.CO;2.

Garrett, T. J., and C. Zhao, 2006: Increased Arctic cloud longwave emissivity associated with pollution from mid-latitudes. *Nature,* **440,** 787–789, doi:10.1038/nature04636.

Haine, T. W., and T. M. Hall, 2002: A generalized transport theory: Water-mass composition and age. *J. Phys. Oceanogr.,* **32,** 1932–1946, doi:10.1175/1520-0485(2002)032<1932:AGTTWM>2.0.CO;2.

Hansen, J., and L. Nazarenko, 2004: Soot climate forcing via snow and ice albedos. *Proc. Natl. Acad. Sci. USA,* **101,** 423–428, doi:10.1073/pnas.2237157100.

Holzer, M., and T. M. Hall, 2000: Transit-time and tracer-age distributions in geophysical flows. *J. Atmos. Sci.,* **57,** 3539–3558, doi:10.1175/1520-0469(2000)057<3539:TTATAD>2.0.CO;2.

——, and G. J. Boer, 2001: Simulated changes in atmospheric transport climate. *J. Climate,* **14,** 4398–4420, doi:10.1175/1520-0442(2001)014<4398:SCIATC>2.0.CO;2.

——, and F. W. Primeau, 2010: Improved constraints on transit time distributions from argon 39: A maximum entropy approach. *J. Geophys. Res.,* **115,** C12021, doi:10.1029/2010JC006410.

——, ——, W. M. Smethie, and S. Khatiwala, 2010: Where and how long ago was water in the western North Atlantic ventilated? Maximum entropy inversions of bottle data from WOCE line A20. *J. Geophys. Res.,* **115,** C07005, doi:10.1029/2009JC005750.

Hoskins, B. J., and K. I. Hodges, 2002: New perspectives on the Northern Hemisphere winter storm tracks. *J. Atmos. Sci.,* **59,** 1041–1061, doi:10.1175/1520-0469(2002)059<1041:NPOTNH>2.0.CO;2.

Houghton, J. T., Y. Ding, D. J. Griggs, M. Noguer, P. J. van der Linden, X. Dai, K. Maskell, and C. A. Johnson, Eds., 2001: *Climate Change 2001: The Scientific Basis*. Cambridge University Press, 881 pp.

Iversen, T., and E. Joranger, 1985: Arctic air pollution and large scale atmospheric flows. *Atmos. Environ.,* **19,** 2099–2108, doi:10.1016/0004-6981(85)90117-9.

Khatiwala, S., F. Primeau, and T. Hall, 2009: Reconstruction of the history of anthropogenic CO_2 concentrations in the ocean. *Nature,* **462,** 346–349, doi:10.1038/nature08526.

——, ——, and M. Holzer, 2012: Ventilation of the deep ocean constrained with tracer observations and implications for radiocarbon estimates of ideal mean age. *Earth Planet. Sci. Lett.,* **325–326,** 116–125, doi:10.1016/j.epsl.2012.01.038.

Klonecki, A., P. Hess, L. Emmons, L. Smith, J. Orlando, and D. Blake, 2003: Seasonal changes in the transport of pollutants into the Arctic troposphere-model study. *J. Geophys. Res.,* **108,** 8367, doi:10.1029/2002JD002199.

Lambert, S. J., and J. C. Fyfe, 2006: Changes in winter cyclone frequencies and strengths simulated in enhanced greenhouse warming experiments: Results from models participating in the IPCC diagnostic exercise. *Climate Dyn.,* **26,** 713–728, doi:10.1007/s00382-006-0110-3.

Law, K. S., and A. Stohl, 2007: Arctic air pollution: Origins and impacts. *Science,* **315,** 1537–1540, doi:10.1126/science.1137695.

Li, Q., and Coauthors, 2005: North American pollution outflow and the trapping of convectively lifted pollution by upper-level anticyclone. *J. Geophys. Res.,* **110,** D10301, doi:10.1029/2004JD005039.

Lin, S.-J., and R. B. Rood, 1996: Multi-dimensional flux-form semi-Lagrangian transport schemes. *Mon. Wea. Rev.,* **124,** 2046–2070, doi:10.1175/1520-0493(1996)124<2046:MFFSLT>2.0.CO;2.

Lu, J., G. A. Vecchi, and T. Reichler, 2007: Expansion of the Hadley cell under global warming. *Geophys. Res. Lett.,* **34,** L06805, doi:10.1029/2006GL028443.

Lubin, D., and A. M. Vogelmann, 2006: A climatologically significant aerosol longwave indirect effect in the Arctic. *Nature,* **439,** 453–456, doi:10.1038/nature04449.

Madonna, E., H. Wernli, H. Joos, and O. Martius, 2014: Warm conveyor belts in the ERA-interim dataset (1979–2010). Part I: Climatology and potential vorticity evolution. *J. Climate,* **27,** 3–26, doi:10.1175/JCLI-D-12-00720.1.

McGrath-Spangler, E., and A. Molod, 2014: Comparison of GEOS-5 AGCM planetary boundary layer depths computed with various definitions. *Atmos. Chem. Phys. Discuss.,* **14,** 6589–6617, doi:10.5194/acpd-14-6589-2014.

Meehl, G. A., C. Covey, K. E. Taylor, T. Delworth, R. J. Stouffer, M. Latif, B. McAvaney, and J. F. Mitchell, 2007: The WCRP CMIP3 multimodel dataset: A new era in climate change research. *Bull. Amer. Meteor. Soc.,* **88,** 1383–1394, doi:10.1175/BAMS-88-9-1383.

Miller, R., G. Schmidt, and D. Shindell, 2006: Forced annular variations in the 20th century Intergovernmental Panel on Climate Change Fourth Assessment Report models. *J. Geophys. Res.,* **111,** D18101, doi:10.1029/2005JD006323.

Mitchell, J., 1957: Visual range in the polar regions with particular reference to the Alaskan Arctic. *J. Atmos. Terr. Phys.,* Suppl. 1, 195–211.

Molod, A., L. Takacs, M. Suarez, J. Bacmeister, I.-S. Song, and A. Eichmann, 2012: The GEOS-5 atmospheric general circulation model: Mean climate and development from MERRA to Fortuna. NASA/TM-2012-104606, Vol 28, 115 pp.

Moore, G., 2012: A new look at Greenland flow distortion and its impact on barrier flow, tip jets and coastal oceanography. *Geophys. Res. Lett.,* **39,** L22806, doi:10.1029/2012GL054017.

——, and I. Renfrew, 2005: Tip jets and barrier winds: A QuikSCAT climatology of high wind speed events around Greenland. *J. Climate,* **18,** 3713–3725, doi:10.1175/JCLI3455.1.

Moorthi, S., and M. J. Suarez, 1992: Relaxed Arakawa–Schubert: A parameterization of moist convection for general circulation models. *Mon. Wea. Rev.,* **120,** 978–1002, doi:10.1175/1520-0493(1992)120<0978:RASAPO>2.0.CO;2.

Neale, R. B., and Coauthors, 2010: Description of the NCAR Community Atmosphere Model (CAM 5.0). NCAR Tech. Note NCAR/TN-486+STR, 274 pp.

Orbe, C., M. Holzer, L. M. Polvani, and D. Waugh, 2013: Air-mass origin as a diagnostic of tropospheric transport. *J. Geophys. Res.,* **118,** 1459–1470, doi:10.1002/jgrd.50133.

Ott, L., S. Pawson, and J. Bacmeister, 2011: An analysis of the impact of convective parameter sensitivity on simulated global atmospheric CO distributions. *J. Geophys. Res.,* **116,** D21310, doi:10.1029/2011JD016077.

Park, M., W. J. Randel, D. E. Kinnison, R. R. Garcia, and W. Choi, 2004: Seasonal variation of methane, water vapor, and nitrogen oxides near the tropopause: Satellite observations and model simulations. *J. Geophys. Res.,* **109,** D03302, doi:10.1029/2003JD003706.

Pawson, S., R. S. Stolarski, A. R. Douglass, P. A. Newman, J. E. Nielsen, S. M. Frith, and M. L. Gupta, 2008: Goddard Earth Observing System Chemistry-Climate Model simulations of stratospheric ozone–temperature coupling between 1950 and 2005. *J. Geophys. Res.,* **113,** D12103, doi:10.1029/2007JD009511.

Raatz, W. E., and G. E. Shaw, 1984: Long-range tropospheric transport of pollution aerosols into the Alaskan Arctic. *J. Climate Appl. Meteor.,* **23,** 1052–1064, doi:10.1175/1520-0450(1984)023<1052:LRTTOP>2.0.CO;2.

Rahn, K. A., and R. J. McCaffrey, 1980: On the origin and transport of the winter Arctic aerosol. *Ann. N. Y. Acad. Sci.,* **338,** 486–503, doi:10.1111/j.1749-6632.1980.tb17142.x.

Randel, W. J., and M. Park, 2006: Deep convective influence on the Asian summer monsoon anticyclone and associated tracer variability observed with Atmospheric Infrared Sounder (AIRS). *J. Geophys. Res.,* **111,** D12314, doi:10.1029/2005JD006490.

Rienecker, M. M., and Coauthors, 2008: The GEOS-5 Data Assimilation System—Documentation of versions 5.0.1, 5.1.0, and 5.2.0. NASA/TM-2008-104606, Vol. 27, 97 pp.

Rosenlof, K. H., A. F. Tuck, K. K. Kelly, J. M. Russell, and M. P. McCormick, 1997: Hemispheric asymmetries in water vapor and inferences about transport in the lower stratosphere. *J. Geophys. Res.,* **102** (D11), 13 213–13 234, doi:10.1029/97JD00873.

Sampe, T., and S.-P. Xie, 2007: Mapping high sea winds from space: A global climatology. *Bull. Amer. Meteor. Soc.,* **88,** 1965–1978, doi:10.1175/BAMS-88-12-1965.

Seidel, D. J., Q. Fu, W. J. Randel, and T. J. Reichler, 2007: Widening of the tropical belt in a changing climate. *Nat. Geosci.,* **1,** 21–24, doi:10.1038/ngeo.2007.38.

Shindell, D., and Coauthors, 2008: A multi-model assessment of pollution transport to the Arctic. *Atmos. Chem. Phys.,* **8,** 5353–5372, doi:10.5194/acp-8-5353-2008.

Sinclair, V. A., S. Gray, and S. Belcher, 2008: Boundary-layer ventilation by baroclinic life cycles. *Quart. J. Roy. Meteor. Soc.,* **134,** 1409–1424, doi:10.1002/qj.293.

Škerlak, B., M. Sprenger, and H. Wernli, 2014: A global climatology of stratosphere–troposphere exchange using the ERA-Interim data set from 1979 to 2011. *Atmos. Chem. Phys.,* **14,** 913–937, doi:10.5194/acp-14-913-2014.

Sprenger, M., and H. Wernli, 2003: A Northern Hemispheric climatology of cross-tropopause exchange for the ERA15 time period (1979–1993). *J. Geophys. Res.,* **108,** 8521, doi:10.1029/2002JD002636.

Stohl, A., 2006: Characteristics of atmospheric transport into the Arctic troposphere. *J. Geophys. Res.,* **111,** D11306, doi:10.1029/2005JD006888.

Tomczak, M., 1981: A multi-parameter extension of TS-diagram techniques for the analysis of non-isopycnal mixing. *Prog. Oceanogr.,* **10,** 147–171, doi:10.1016/0079-6611(81)90010-0.

von Engeln, A., and J. Teixeira, 2013: A planetary boundary layer height climatology derived from ECMWF reanalysis data. *J. Climate,* **26,** 6575–6590, doi:10.1175/JCLI-D-12-00385.1.

Wang, S., E. P. Gerber, and L. M. Polvani, 2012: Abrupt circulation responses to tropical upper-tropospheric warming in a relatively simple stratosphere-resolving AGCM. *J. Climate,* **25,** 4097–4115, doi:10.1175/JCLI-D-11-00166.1.

WMO, 2007: Scientific assessment of ozone depletion: 2006. Global Ozone Research and Monitoring Project Rep. 50, World Meteorological Organization, 572 pp.

Wu, Y., M. Ting, R. Seager, H.-P. Huang, and M. A. Cane, 2011: Changes in storm tracks and energy transports in a warmer climate simulated by the GFDL CM2.1 model. *Climate Dyn.,* **37,** 53–72, doi:10.1007/s00382-010-0776-4.

Yin, J. H., 2005: A consistent poleward shift of the storm tracks in simulations of 21st century climate. *Geophys. Res. Lett.,* **32,** L18701, doi:10.1029/2005GL023684.